LIGHT SCATTERING FROM

MICRON SIZED PARTICLES

By

ULF NOBBMANN

Bachelor of Science

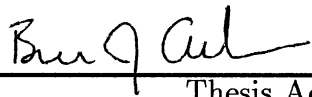University of Hannover

Hannover, Germany

1988

Submitted to the Faculty of the
Graduate College of the
Oklahoma State University
in partial fulfillment of
the requirements for
the Degree of
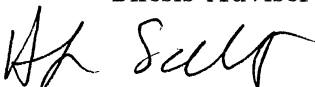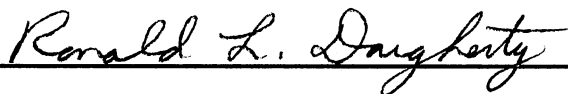MASTER OF SCIENCE
December, 1991

Thesis
1991
N744L

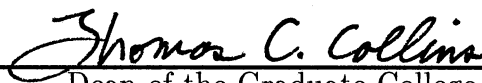# LIGHT SCATTERING FROM
MICRON SIZED PARTICLES

Thesis Approved:

Bru J Aul
Thesis Adviser

Hh Salt

Ronald L. Daugherty

Thomas C. Collins
Dean of the Graduate College

ACKNOWLEDGMENTS

I would also like to express my gratitude to my 'Professoren und Kommilitonen' in Hannover who didn't scare me away from physics.

The biggest thanks are due now: to my parents, my sister and the other members of our family. Without their support and encouragement, this whole adventure would not have taken place. It wouldn't have been worth it without those letters and packages keeping me up to date...

Vielen Dank an alle !

TABLE OF CONTENTS

LIST OF TABLES

LIST OF FIGURES

CHAPTER I

INTRODUCTION

The scattering of light began to interest men long ago. Science has since demystified several natural phenomena like the blue color of the sky, the colors of the sunset, rainbow, glory, corona and halo to be due to scattering by air molecules, water droplets, aerosols and ice crystals. All previous phenomena can be generalized to scattering by colloids. The area of colloidal science has grown to a large field since its foundation which is usually connected with Brown (pollen in water, 1829, [1,2]) and Tyndall (scattering by aerosols, [3,4]) , to name but a few of the large list of contributors to its advancement. Today light scattering from colloids is used in chemistry, physics, biochemistry, medicine and engineering to study materials, in particular solutions of macromolecules [5]. The most interest has been put on the investigation of particles with radii between 1 nm and 1 μm; the lower limit being due to the constraint that the scattering objects have to be significantly larger than the solvent molecules, the upper limit ensuring the dominance of the particles' Brownian motion over gravitational or convection effects [6]. To investigate the scattering from a collection of different particle sizes and shapes one first has to understand what contributions come from the different members of the scattering sample. The easiest system contains only exact spheres of one size. Ideally this can never be realized. However synthetic colloids were first made in the 1940's, and now the variations in the properties of the individual members of a scattering ensemble are small. To determine the quality of a particular sample, its scattering has to be compared to the expected result of a perfect model system. In this work several synthetic colloidal spheres, made by

well-established methods, were characterized by light scattering. Measurements of the average mean intensity were compared to modified RDG form factors [7]. The observed dependence of the diffusion constant obtained by a cumulant fit to the intensity autocorrelation function suggested that a different particle size distribution model — other than the most commonly used Schulz distribution [8] — might explain the deviations.

Previous Work in the Field

The work of this thesis has many similarities to the work done by Pusey and van Megen on the detection of small polydispersities [9]. They investigated the effects of polydispersity on Schulz distributions of spheres. A predecessor to their paper was a theoretical study of dynamic light scattering on polydisperse systems by Aragón and Pecora [10], who showed applicability to spherical, ellipsoidal, and Gaussian coil particles. Numerical results for polydisperse rods and Gaussian coils were reported by Tagami and Pecora [11] where a Schulz distribution of molecular weights was used in the calculations. The possibility to model polydispersity with a Schulz distribution was confirmed by Kotlarchyk, Stephens, and Huang [12]. They found that it was an appropriate choice for a particle distribution. It explained the small-angle neutron scattering results of a model water-in-oil three-component microemulsion, but they noticed a consistent shoulder of their data on the large side of the Schulz distribution. Mazer, Benedek, and Carey —contrary to the previous references— could not support the Schulz distribution: rod like micelles of Sodium Dodecyl Sulfate in aqueous sodium chloride solutions showed no angular dependance of the mean diffusion coefficient obtained from dynamic light scattering in spite of a large polydispersity[13]. They analyzed their data using the method of cumulants [14]. Van Megen, Ottewill, Owens, and Pusey report angle dependence of the free particle diffusion constant for PMMA particles [15]. They also look at concentrated samples where structure factors and hydrodynamic interactions enter the stage. Several publications discuss the effect of concentration on the effective diffusion constant; a wide array of different samples is covered: polystyrene in

water [16,17], polystyrene in cyclohexane [18], PMMA [19], silica [20–22], theory only [23,24]). Brehm and Bloomfield observed a decrease in the apparent size with increasing scattering angles, they investigated a bimodal mix of small and very small latex particles [25]. Since Schmidt, Burchard, and Ford use larger polytstyrene they can report a minimum in the apparent size as a function of the wave vector [26].

This thesis reports extrema in the apparent size versus scattering angle as well, only here maxima instead of minima occur, and not only the first maximum is considered.

CHAPTER II

THEORY

In this chapter the scattering of light by independent spherical particles will be described. Although it is possible to write down the exact solution of the scattering of a plane electromagnetic wave by an isotropic, homogeneous sphere of arbitrary size, this path is not taken. The references provide a detailed explanation of the steps involved. The results of those calculations will be used instead. However it is helpful to define some quantities and expressions before the results appear.

If a wave with incident wave vector $\vec{k}_i$ gets scattered into a new direction, the scattered wave is described by the scattered wave vector $\vec{k}_s$. The magnitude of the wave vectors is given by

$$k_{i \atop s} = |\vec{k}_{i \atop s}| = \frac{2\pi n}{\lambda_{i \atop s}} \ , \tag{1}$$

where n is the index of refraction of the medium and $\lambda_{i \atop s}$ is the wavelength *in vacuo* of the light before and after the scattering. The momentum of an incident photon is $\hbar \vec{k}_i$ and the momentum of the scattered photon is then $\hbar \vec{k}_s$. The difference of these vectors is the momentum transfer

$$\hbar \vec{q} = \hbar(\vec{k}_i - \vec{k}_s) \ . \tag{2}$$

In elastic scattering no energy is absorbed; the wavelength before and after the scattering does not change. Under that assumption:

$$|\vec{k}_i| = |\vec{k}_s| =: k \ , \tag{3}$$

where the index on the k is dropped for easier reading. Applying this equation to the relation for $q = |\vec{q}|$ produces

$$q = 4k^2 \sin\left(\frac{\theta}{2}\right) = \frac{4\pi n}{\lambda} \sin\left(\frac{\theta}{2}\right) \ . \tag{4}$$

4

The scattering angle θ is formed by the incident and the scattered wave vectors. An incident plane electromagnetic wave is described by [27,28]

$$\vec{E}_i = \vec{E}_0 \exp i(\vec{k}_i \cdot \vec{r} - \omega t) \ , \tag{5}$$

where ω is the circular frequency of the incident radiation and $\vec{E}_0$ is the amplitude of the electric field. If this field induces a dipole in an object placed at the origin with the refractive index n_{obj} the scattered field will obey the following expression:

$$\vec{E}_s \propto \vec{E}_0 \frac{k^2}{R} \frac{m^2 - 1}{m^2 + 2} \exp i(\vec{k}_s \cdot \vec{R} - \omega t) \ . \tag{6}$$

Here m is the ratio of the refractive indices of the scattering object and the surrounding medium, $\frac{n_{obj}}{n_{med}}$. For this to be valid, $\vec{E}_0$ has to be perpendicular to the scattering plane defined by the two vectors $\vec{k}_i$ and $\vec{k}_s$, and the field has to be measured at a large distance R from the origin, the location of the scattering object. Since the scattered intensity is proportional to $|\vec{E}_s|^2$, it can be written as [7,29]

$$I(k, R) \propto \frac{|\vec{E}_0|^2 k^4}{R^2} \left(\frac{m^2 - 1}{m^2 + 2}\right)^2 \ . \tag{7}$$

The intensity increases with k^4 which explains the blue color of the sky: Shorter wavelengths (blue) are scattered more strongly in the atmosphere of the earth than longer wavelengths (red). For sunsets the effect is reversed: The light arrives after more blue light has been scattered out of the incident direction than red light. Thus at dusk and dawn the sky 'in the vicinity' of the sun looks red [30,31]. Multiple scattering, colloidal particles in the atmosphere, and nonspherical molecules make the explanation of the colors of the sky more complicated. The decrease of the scattered intensity with R^2 is instructive: The area of a sphere surrounding the dipole scatterer increases with the square of its radius. Equation 7 was found by Rayleigh. In the above description no time dependence influenced the results. For that reason the study of the scattered intensity is also called "Static Light Scattering".

The fluctuations of the scattered intensity with time are examined in Dynamic Light Scattering. Here one measures the intensity correlation function defined by [32]

$$g^2(\vec{r},\vec{k},\tau) := \frac{< I(\vec{r},\vec{k},t) \cdot I(\vec{r},\vec{k},t+\tau) >}{< I(\vec{r},\vec{k},t) >< I(\vec{r},\vec{k},t) >} \quad , \tag{8}$$

where τ is called delay time and the average $<>$ denotes the ensemble average. For the auto correlation function – the convolution of the intensity with itself – this gives:

$$< I(t)I(t+\tau) >= \lim_{t_{\text{dur}} \to \infty} \frac{1}{t_{\text{dur}}} \int_0^{t_{\text{dur}}} I(t)I(t+\tau)\,dt \approx \sum_{i=1}^{N-(\tau/\delta\tau)} I(t_i)I(t_i+\tau) \quad , \tag{9}$$

where t_{dur} is the duration of the measurement to determine the time average. The sum $\sum_{i=1}^{N-(\tau/\delta\tau)}$ is the experimental realization of this average. The spacing between the measurements is

$$\delta\tau = t_{i+1} - t_i \quad . \tag{10}$$

The intensity is measured at N equally spaced time intervals , each value is multiplied by the measured value at the time $t_i + \tau = t_{i+(\tau/\delta\tau)}$ and this is added up over the duration of the experiment $N \cdot \tau$. Another way of describing the randomness of the scattered signal is the field autocorrelation function defined by [33]

$$g^1(\vec{r},\vec{k},\tau) := \frac{< E(\vec{r},\vec{k},t) \cdot E^*(\vec{r},\vec{k},t+\tau) >}{< E(\vec{r},\vec{k},t) >^2} \quad , \tag{11}$$

where E^* is the complex conjugate of the electric field E . For Gaussian light the intensity correlation function (Equation 8) and the field correlation function are not independent:

$$g^2(\vec{r},\vec{k},\tau) = 1 + \gamma|g^1(\vec{r},\vec{k},\tau)|^2 \quad . \tag{12}$$

This equation is also called Siegert relation after its discoverer [34]. The coefficient γ is a constant related to the signal to noise ratio of the particular setup of the experiment [33,35].

A dipole at the origin scatters light that can be described by Equation 6. The expression is slightly modified if that dipole is placed at the location $\vec{r}$ with

$|\vec{r}| \ll \vec{R}$:

$$\vec{E}_s \propto \vec{E}_0 \frac{k^2}{R} \frac{m^2 - 1}{m^2 + 2} \exp\left(ikR\right) \exp i(\vec{q} \cdot \vec{r} - \omega t) \; , \tag{13}$$

where the exponential $\vec{k}_s \cdot \vec{R}$ from Equation 6 is here $k_s \cdot |\vec{R} - \vec{r}|$ which can be expanded to yield the result. Inserting Equation 13 into Equation 11 yields

$$g^1(\vec{q}, \tau) = < \exp i(\vec{q} \cdot (\vec{r}(t + \tau) - \vec{r}(t))) > \; . \tag{14}$$

This average can also be calculated with an integral

$$g^1(\vec{q}, \tau) = \int_{\text{all space}} \exp\left(i\vec{q} \cdot \vec{\delta r}\right) P(\vec{\delta r}, \tau)\, d^3\vec{\delta r} \; , \tag{15}$$

where $P(\vec{\delta r}, \tau)$ denotes the normalized probability of finding a particle displaced by the vector $\vec{\delta r}$ after the time τ has elapsed. This probability function has to satisfy a diffusion equation:

$$\frac{\partial}{\partial \tau} P(\vec{\delta r}, \tau) = D\vec{\nabla}^2 P(\vec{\delta r}, \tau) \; , \tag{16}$$

where D is the diffusion constant of the particle. Transforming this equation from real space into Fourier space is equivalent to replacing $\vec{\nabla}$ by $i\vec{q}$:

$$\frac{\partial}{\partial \tau} \tilde{P}(\vec{q}, \tau) = -Dq^2 \tilde{P}(\vec{q}, \tau) \; . \tag{17}$$

The function $\tilde{P}(\vec{q}, \tau)$ is the Fourier transform of $P(\vec{r}, \tau)$:

$$\tilde{P}(\vec{q}, \tau) = \int_{\text{all space}} P(\vec{r}, \tau) \exp\left(i\vec{q} \cdot \vec{r}\right) d^3\vec{r} \; . \tag{18}$$

Equation 17 is easily solved since the derivative of the unknown function is proportional to itself:

$$\tilde{P}(\vec{q}, \tau) = \exp\left(-Dq^2\tau\right) \; . \tag{19}$$

If the variable $\vec{\delta r}$ in Equation 15 is renamed $\vec{r}$, Equation 18 is obtained. This implies that

$$g^1(\vec{q}, \tau) = \tilde{P}(\vec{q}, \tau) = \exp\left(-Dq^2\tau\right) \; , \tag{20}$$

which is the field autocorrelation function for a particle diffusing with the diffusion constant D.

Scattering from Spheres

In the Rayleigh-Debye-Gans approximation, the scattering particles are assumed to consist of individual non-interfering dipoles. This approximation is valid if the difference between the refractive index of the medium and of the scattering object is significantly smaller than the ratio of the wavelength to the size a of the scattering object:

$$(n_{obj} - n_{med}) \ll \frac{\lambda}{a} \ . \tag{21}$$

This can equivalently be expressed as [7]

$$2ka(m - 1) \ll 1 \ . \tag{22}$$

With this assumption, the evaluation of the field scattered by a particle becomes a volume integral over the fields scattered by each individual dipole in the particle.

Static Light Scattering

The field scattered by a dipole was (Equation 13) :

$$\vec{E}_s \propto \vec{E}_0 \frac{k^2}{R} \frac{m^2 - 1}{m^2 + 2} \exp\left(ikR\right) \exp i(\vec{q} \cdot \vec{r} - \omega t) \ .$$

Under Rayleigh-Gans-Debye assumptions, the total field scattered by a sphere of radius a becomes:

$$
\begin{aligned}
\vec{E}_{total} &= \int_{volume\ of\ sphere} \vec{E}_s\, d^3\vec{r} = \int_0^{4\pi} \int_0^a \vec{E}_s r^2\, dr\, d\Omega \\
&\propto \int_0^{4\pi} \int_0^a \vec{E}_0 \frac{k^2}{R} \frac{m^2 - 1}{m^2 + 2} \exp\left(ikR\right) \exp i(\vec{q} \cdot \vec{r} - \omega t)\, r^2\, dr\, d\Omega \\
&\propto \vec{E}_0 \frac{k^2}{R} \frac{m^2 - 1}{m^2 + 2} \exp\left(ikR\right) \exp\left(-i\omega t\right) 2\pi \int_{-1}^1 \int_0^a \exp\left(i\vec{q} \cdot \vec{r}\right) r^2\, dr\, d(\cos\alpha) \\
&\propto \int_{-1}^1 \int_0^a \exp\left(i\vec{q} \cdot \vec{r}\right) r^2\, dr\, d(\cos\alpha) \ . \tag{23}
\end{aligned}
$$

The angle α is formed by the vectors $\vec{q}$ and $\vec{r}$, the integration variable Ω is the solid angle. The integral in Equation 23 can be performed:

$$\int_{-1}^1 \int_0^a \exp\left(i\vec{q} \cdot \vec{r}\right) r^2\, dr\, d(\cos\alpha) = \frac{3}{q^3}\left(\sin\left(qa\right) - qa\cos\left(qa\right)\right) \ . \tag{24}$$

The scattered intensity is proportional to the square of this expression[7]:

$$I(q) = I_0 \frac{9}{q^6}(\sin{(qa)} - qa\cos{(qa)})^2 \ , \tag{25}$$

I_0 is the proportionality constant describing the amplitude of the intensity. This equation is more often written as

$$I(q) = I_0 a^6 P(qa) \ , \tag{26}$$

where

$$P(qa) = \frac{9}{(qa)^6}(\sin{(qa)} - qa\cos{(qa)})^2 \tag{27}$$

is called the form factor of a sphere. This form factor is normalized, the intercept of this function is $P(qa = 0) = 1$. P varies over several orders of magnitude and shows minima and maxima depending on the qa–range available. The first minimum occurs at $qa = 4.49$. (The positions of the minima are determined by the transcendental equation $\tan{(qa)} = qa$.) This minimum can not be observed by light scattering from small particles (radius $\lesssim$ 200 nm). For very small particles the form factor can be approximated to $P(qa) \approx 1 - \frac{1}{5}(qa)^2 = 1 - \frac{1}{3}(qR_G)^2$. The last equality is valid for spheres with a radius of gyration R_G [36]. This expression is widely used to determine molecular weights of macromolecules by plotting the scattered intensity versus q^2 [37,38].

Dynamic Light Scattering

In Dynamic Light Scattering, the correlation function of the scattered light is measured. For the field correlation function, the general result was given in Equation 20 :

$$g^1(\vec{q}, \tau) = \exp{(-Dq^2\tau)} \ ,$$

where D is the diffusion constant of the particles examined. For a perfect sphere of radius a, this diffusion constant was found by Einstein [39]:

$$D = \frac{k_B T}{6\pi\eta a} \ , \tag{28}$$

where k_B is the Boltzmann constant, T is the absolute temperature, and η is the viscosity of the medium through which the sphere is diffusing. The diffusion constant is the ratio of the thermal driving force $k_B T$ and $6\pi\eta a$ is related to the viscous drag. With the expression for D, the field correlation function becomes

$$g^1(\vec{q},\tau) = \exp\left(-\frac{k_B T}{6\pi\eta a}q^2\tau\right) \ . \tag{29}$$

This result is only valid for samples with particles that are uniform in size. It is the solution for monodisperse spheres. In the next section, the more realistic assumption of a collection of different sphere sizes is described.

A Collection of Different Spheres

The distribution of particle radii can be described by a probability function $G(a)$. The function $G(a)$ says how many spheres of radius a can be found in the sample. It is convenient to normalize this function by demanding that

$$\int_0^\infty G(a)\, da = 1 \ . \tag{30}$$

Then all values of this function will be smaller than or equal to 1 :

$$\forall a \ \ G(a) \leq 1 \ .$$

Under these conditions $G(a)$ gives the fraction of particles with radius a.

Static Light Scattering

Each sphere of the collection of spheres scatters light according to Equation 27 :

$$P(qa) = \frac{9}{(qa)^6}(\sin(qa) - qa\cos(qa))^2 \ .$$

To get the scattering from the whole ensemble, the scattering from each member has to be added up [9]:

$$I(q) = I_0 \int_0^\infty a^6 P(qa)G(a)\, da \ , \tag{31}$$

where Equation 26 has been used. This procedure is almost the same for the dynamic scattering.

Dynamic Light Scattering

According to Equation 28 each sphere has the diffusion constant:

$$D(a) = \frac{k_B T}{6\pi\eta a} \quad .$$

The measured correlation function contains decays of the whole ensemble. The effective diffusion constant of the collection of spheres will be the intensity weighted average diffusion constant, because dynamic light scattering detects intensity fluctuations and different sizes contribute with different (Equation 26) strengths. Thus the effective diffusion constant is [9]:

$$D_{\text{eff}}(q) = \frac{\int_0^\infty D(a) I_0 a^6 P(qa) G(a)\, da}{I(q)} \quad , \tag{32}$$

and the field correlation function is then:

$$g^1(\vec{q}, \tau) = \exp\left(-D_{\text{eff}}(q) q^2 \tau\right) \quad . \tag{33}$$

In the following chapter, a special particle distribution is investigated. For the case of that size distribution, the integrals in Equation 31 and in Equation 32 can be evaluated analytically.

CHAPTER III

POLYDISPERSE SAMPLES

The previous chapter described the interactions of monodisperse spheres. Each sphere in a sample is assumed to have exactly the same radius. However this situation can not be found in nature. Particles always have a certain spread in sizes. The width of the particle distribution might be very small, yet it is impossible to find or produce particles with a delta function as the particle size distribution. Several distributions have been used to model polydisperse samples. It has been reported that the detailed shape of the distribution does not influence the results significantly [40]. For that reason the Schulz or generalized exponential distribution is chosen frequently. This function is mathematically easier to handle. Integrals containing this function can be evaluated analytically by repeated integration by parts.

The Schulz Distribution

The generalized exponential or Schulz distribution is [8]:

$$G_Z(a) = \frac{a^Z}{Z!}(\frac{Z+1}{\overline{a}})^{Z+1} \exp\left(-\frac{a}{\overline{a}}(Z+1)\right) ,$$ (34)

where Z is a parameter related to the polydispersity and $\overline{a}$ is the first order or number averaged radius of this distribution (sometimes also called first moment). The function $G_Z(a)$ is normalized:

$$\int_0^\infty G_Z(a)\, da = 1 .$$ (35)

The n-th moment [9] is given by

$$\overline{a^n} = \int_0^\infty G_Z(a)a^n \, da .$$ (36)

The polydispersity σ is the relative standard deviation of the distribution [9]:

$$\sigma = (\frac{1}{Z+1})^{\frac{1}{2}} \ . \tag{37}$$

A small Z thus refers to a large polydispersity. For very large Z, the functional form of $G_Z(a)$ asymptotically approaches a Gaussian. $G_Z(a)$ shows asymmetry towards larger sizes for small values of Z, i. e. the function is not symmetric about its maximum. There are more particles with larger radii ('left of the maximum') than particles with smaller radii ('right of the maximum').

The form factor given in Equation 27 can be rewritten as

$$P(qa) = \frac{9}{2(qa)^6}(1 + (qa)^2 - 2qa\sin(2qa) - \cos(2qa) + (qa)^2\cos(2qa)) \tag{38}$$

by using trigonometric identities. With this form factor, integrals of the following kind will appear in calculations for the scattering from an ensemble of different particle sizes [9]:

$$I_n = \int_0^\infty G(a)(qa)^n \, da \ , \tag{39}$$

$$C_n = \int_0^\infty G(a)(qa)^n \cos(2qa) \, da \ , \tag{40}$$

$$S_n = \int_0^\infty G(a)(qa)^n \sin(2qa) \, da \ . \tag{41}$$

For a Schulz distribution, these integrals can be solved analytically. The derivation of the integrals is given in Appendix A. The results are [9]:

$$I_n = (\frac{q\bar{a}}{Z+1})^n \frac{(Z+n)!}{Z!} \ , \tag{42}$$

$$C_n = I_n(1 + (\frac{2q\bar{a}}{Z+1})^2)^{-\frac{Z+n+1}{2}} \cos\left\{(Z+n+1)\arctan(\frac{2q\bar{a}}{Z+1})\right\} \ , \tag{43}$$

$$S_n = I_n(1 + (\frac{2q\bar{a}}{Z+1})^2)^{-\frac{Z+n+1}{2}} \sin\left\{(Z+n+1)\arctan(\frac{2q\bar{a}}{Z+1})\right\} \ . \tag{44}$$

The static and dynamic scattering results can now be expressed in terms of these integrals I_n, C_n, and S_n .

Static Scattering

Equation 31 described the static scattering for a general collection of spheres:

$$I(q) = I_0 \int_0^\infty a^6 P(qa) G(a) \, da \ .$$

Since the particle distribution is given by Equation 34, the intensity becomes:

$$I(q) = I_0 \int_0^\infty a^6 P(qa) G_Z(a) \, da \ . \tag{45}$$

It is convenient to normalize the intensity by dividing this expression by the $q \to 0$ limit

$$I(0) = \lim_{q \to 0} I_0 \int_0^\infty a^6 P(qa) G_Z(a) \, da = I_0 \overline{a^6} \ , \tag{46}$$

where Equation 36 and the relation

$$\lim_{q \to 0} P(qa) = 1$$

were used. Thus the normalized intensity is

$$\frac{I(q)}{I(0)} = \frac{1}{\overline{a^6}} \int_0^\infty a^6 P(qa) G_Z(a) \, da \ . \tag{47}$$

The relation of Equation 38 can be inserted and reduces the integral to a sum of integrals which can be evaluated [9]:

$$\frac{I(q)}{I(0)} = \frac{9}{2q^6 \overline{a^6}} (1 + C_2 - 2S_1 - C_0 + I_2) \ , \tag{48}$$

where according to Equations 42 – 44 :

$$C_0 = (1 + (\frac{2q\overline{a}}{Z+1})^2)^{-\frac{Z+1}{2}} \cos\left\{ (Z+1) \arctan\left(\frac{2q\overline{a}}{Z+1}\right) \right\} \ , \tag{49}$$

$$S_1 = q\overline{a}(1 + (\frac{2q\overline{a}}{Z+1})^2)^{-\frac{Z+2}{2}} \sin\left\{ (Z+2) \arctan\left(\frac{2q\overline{a}}{Z+1}\right) \right\} \ , \tag{50}$$

$$S_1 = q\overline{a}(1 + (\frac{2q\overline{a}}{Z+1})^2)^{-\frac{Z+2}{2}} \sin\left\{ (Z+2) \arctan\left(\frac{2q\overline{a}}{Z+1}\right) \right\} \ , \tag{51}$$

$$I_2 = q^2 \overline{a^2} = \frac{q^2 \overline{a}^2 (Z+2)}{Z+1} \ , \tag{52}$$

$$C_2 = q^2 \overline{a^2}(1 + (\frac{2q\overline{a}}{Z+1})^2)^{-\frac{Z+3}{2}} \cos\left\{ (Z+3) \arctan\left(\frac{2q\overline{a}}{Z+1}\right) \right\} \ . \tag{53}$$

Dynamic Scattering

Equation 32 described the dynamic scattering for a general distribution of spheres:

$$D_{eff}(q) = \frac{\int_0^\infty D(a)I_0 a^6 P(qa)G(a)\,da}{I(q)} \quad .$$

Now the Schulz distribution (Equation 34) can be inserted:

$$D_{eff}(q) = \frac{\int_0^\infty D(a)I_0 a^6 P(qa)G_Z(a)\,da}{I(q)} \quad . \tag{54}$$

The size resulting from the measurement of this diffusion constant is inversely proportional to $D_{eff}(q)$. It is again convenient to calculate a normalized expression. The normalized apparent size is given by the ratio $D_{eff}(0)/D_{eff}(q)$. $D_{eff}(0)$ is the $q \to 0$ limit of $D_{eff}(q)$:

$$D_{eff}(0) = \lim_{q\to 0} \frac{\int_0^\infty D(a)I_0 a^6 P(qa)G_Z(a)\,da}{I(q)} = \frac{k_B T}{6\pi\eta}\frac{\overline{a^5}}{\overline{a^6}} \quad , \tag{55}$$

where Equations 28 and 46 have been applied to find the limit. Inserting Equation 38 into Equation 54, the normalized apparent size becomes [9]:

$$\frac{D_{eff}(0)}{D_{eff}(q)} = \frac{\overline{a^5}}{q\overline{a^6}}\frac{1 + C_2 - 2S_1 - C_0 + I_2}{I_{-1} + I_1 - 2S_0 - C_{-1} + C_1} \quad , \tag{56}$$

where according to Equations 42 − 44 :

$$I_{-1} = \frac{Z+1}{q\overline{a}Z} \quad , \tag{57}$$

$$I_1 = q\overline{a} \quad , \tag{58}$$

$$S_0 = (1 + (\frac{2q\overline{a}}{Z+1})^2)^{-\frac{Z+1}{2}} \sin\left\{(Z+1)\arctan(\frac{2q\overline{a}}{Z+1})\right\} \quad , \tag{59}$$

$$C_{-1} = \frac{Z+1}{q\overline{a}Z}(1 + (\frac{2q\overline{a}}{Z+1})^2)^{-\frac{Z}{2}} \cos\left\{Z\arctan(\frac{2q\overline{a}}{Z+1})\right\} \quad , \tag{60}$$

$$C_1 = q\overline{a}(1 + (\frac{2q\overline{a}}{Z+1})^2)^{-\frac{Z+2}{2}} \cos\left\{(Z+2)\arctan(\frac{2q\overline{a}}{Z+1})\right\} \quad , \tag{61}$$

and C_2, $2S_1$, C_0, and I_2 are given by Equations 49 − 53. For the following modified Schulz distributions, the calculations are very similar. Instead of one generalized exponential distribution, the sum of two such distributions will be considered.

Modified Schulz Distribution

The previous section contains results produced by a distribution of particle sizes according to (Equation 34):

$$G_Z(a) = \frac{a^Z}{Z!}(\frac{Z+1}{\bar{a}})^{Z+1} \exp\left(-\frac{a}{\bar{a}}(Z+1)\right) \; .$$

This equation describes a collection of spheres with the 'prevalent' size around $\bar{a}$. What happens if there are two peaks in the size distribution? This case is equivalent to a sum of two different Schulz distributions with different sets of parameters:

$$G_{mod}(a) = \beta_1 G_{Z_1,R_1}(a) + \beta_2 G_{Z_2,R_2}(a) \; , \tag{62}$$

where the two normalized contributors are

$$G_{Z_i,R_i}(a) = \frac{a^{Z_i}}{Z_i!}(\frac{Z_i+1}{\overline{R_i}})^{Z_i+1} \exp\left(-\frac{a}{\overline{R_i}}(Z_i+1)\right) \;, i = 1,2 \tag{63}$$

and the two parameters β_1 and β_2 are not independent because normalization of the function $G_{mod}(a)$ results in the constraint

$$\int_0^\infty G_{mod}(a)\,da = \beta_1 + \beta_2 \overset{!}{=} 1 \; , \tag{64}$$

where the normalization of $G_{Z_i,R_i}(a)$ was used to evaluate the integral. The n-th moment of the two distributions $G_{Z_1,R_1}(a)$ and $G_{Z_2,R_2}(a)$ will be denoted $\overline{R_1^n}$ and $\overline{R_2^n}$ respectively:

$$\overline{R_i^n} = \int_0^\infty G_{Z_i,R_i}(a)a^n\,da \;, i = 1,2 \; . \tag{65}$$

Static Scattering

The wave vector dependence of the intensity (see Equation 31) is with the distribution of Equation 62:

$$I(q) = I_0 \int_0^\infty a^6 P(qa)G_{mod}(a)\,da \; .$$

After finding the $q \to 0$ limit

$$I(0) = \lim_{q\to 0} I_0 \int_0^\infty a^6 P(qa)G_{mod}(a)\,da = I_0(\beta_1\overline{R_1^6} + \beta_2\overline{R_2^6}) \; , \tag{66}$$

the normalized intensity can be written as:

$$\frac{I(q)}{I(0)} =$$

$$\frac{9}{2q^6} \cdot \left\{ \beta_1 \frac{1 + C_2(Z_1, R_1) - 2S_1(Z_1, R_1) - C_0(Z_1, R_1) + I_2(Z_1, R_1)}{\beta_1 \overline{R_1^6} + \beta_2 \overline{R_2^6}} \right.$$

$$\left. + \beta_2 \frac{1 + C_2(Z_2, R_2) - 2S_1(Z_2, R_2) - C_0(Z_2, R_2) + I_2(Z_2, R_2)}{\beta_1 \overline{R_1^6} + \beta_2 \overline{R_2^6}} \right\} , \quad (67)$$

where Equations 38 , 62 and 66 have been applied. Here the integrals are calculated using Equations 42 – 44 with the appropriate corrections, i. e. replacing Z and $\overline{a}$ with $Z_{1/2}$ and $\overline{R_{1/2}}$ respectively. They are for $i = 1, 2$:

$$C_0(Z_i, R_i) = (1 + (\frac{2q\overline{R_i}}{Z_i + 1})^2)^{-\frac{Z_i + 1}{2}} \cos \left\{ (Z_i + 1) \arctan (\frac{2q\overline{R_i}}{Z_i + 1}) \right\} , \quad (68)$$

$$S_1(Z_i, R_i) = q\overline{R_i}(1 + (\frac{2q\overline{R_i}}{Z_i + 1})^2)^{-\frac{Z_i + 2}{2}} \sin \left\{ (Z_i + 2) \arctan (\frac{2q\overline{R_i}}{Z_i + 1}) \right\} , \quad (69)$$

$$S_1(Z_i, R_i) = q\overline{R_i}(1 + (\frac{2q\overline{R_i}}{Z_i + 1})^2)^{-\frac{Z_i + 2}{2}} \sin \left\{ (Z_i + 2) \arctan (\frac{2q\overline{R_i}}{Z_i + 1}) \right\} , \quad (70)$$

$$I_2(Z_i, R_i) = q^2\overline{a^2} = \frac{q^2\overline{R_i}^2(Z_i + 2)}{Z_i + 1} , \quad (71)$$

and

$$C_2(Z_i, R_i) = q^2\overline{a^2}(1 + (\frac{2q\overline{R_i}}{Z_i + 1})^2)^{-\frac{Z_i + 3}{2}} \cos \left\{ (Z_i + 3) \arctan (\frac{2q\overline{R_i}}{Z_i + 1}) \right\} . \quad (72)$$

These equations are of course very similar to Equations 49 – 53. The average $\overline{R_{1/2}^6}$ can be calculated with Equation 42:

$$\overline{R_1^6} = \frac{I_6(Z_1, R_1)}{q^6} = \overline{R_1}^6 \frac{(Z_1 + 6)(Z_1 + 5)(Z_1 + 4)(Z_1 + 3)(Z_1 + 2)}{(Z_1 + 1)^5} , \quad (73)$$

and equivalently

$$\overline{R_2^6} = \frac{I_6(Z_2, R_2)}{q^6} = \overline{R_2}^6 \frac{(Z_2 + 6)(Z_2 + 5)(Z_2 + 4)(Z_2 + 3)(Z_2 + 2)}{(Z_2 + 1)^5} .$$

With these expressions the result of Equation 67 can be rewritten as :

$$\frac{I(q)}{I(0)} =$$

$$\frac{9}{2}\Big\{1+\kappa(1+C_2(Z_1,R_1)-2S_1(Z_1,R_1)-C_0(Z_1,R_1)+I_2(Z_1,R_1))$$

$$+(1+C_2(Z_2,R_2)-2S_1(Z_2,R_2)-C_0(Z_2,R_2)+I_2(Z_2,R_2))\Big\}$$

$$\div\Big\{\kappa(q\overline{R_1})^6\frac{(Z_1+6)(Z_1+5)(Z_1+4)(Z_1+3)(Z_1+2)}{(Z_1+1)^5}$$

$$+(q\overline{R_2})^6\frac{(Z_2+6)(Z_2+5)(Z_2+4)(Z_2+3)(Z_2+2)}{(Z_2+1)^5}\Big\}\ , \tag{74}$$

where the condition $\beta_1+\beta_2=1$ and the definition

$$\kappa:=\frac{\beta_1}{\beta_2} \tag{75}$$

are used. Equation 74 was used to obtain fits to the static scattering data. The parameters $Z_{1/2}$, $R_{1/2}$, κ, and the amplitude $I(0)$ were varied until the expected $I(q)$ agreed well with the measured intensities.

Dynamic Scattering

The effective diffusion coefficient was defined in Equation 32. Here the particles are described by Equation 62. This yields the diffusion coefficient to be:

$$D_{eff}(q)=\frac{\int_0^\infty D(a)I_0 a^6 P(qa)G_{mod}(a)\,da}{I(q)}\ .$$

The $q\to 0$ limit of this expression is:

$$D_{eff}(0)=\lim_{q\to 0}\frac{\int_0^\infty D(a)I_0 a^6 P(qa)G_{mod}(a)\,da}{I(q)}=\frac{k_B T}{6\pi\eta}\frac{\beta_1\overline{R_1^5}+\beta_2\overline{R_2^5}}{\beta_1\overline{R_1^6}+\beta_2\overline{R_2^6}}\ . \tag{76}$$

The normalized apparent size is $D_{eff}(0)/D_{eff}(q)$, or more explicitly after using Equations 38, 62 and 76 and performing the integrations:

$$\frac{D_{eff}(0)}{D_{eff}(q)}=$$

$$\frac{\beta_1\overline{R_1^5}+\beta_2\overline{R_2^5}}{\beta_1 q\overline{R_1^6}+\beta_2 q\overline{R_2^6}}\Big\{\beta_1(1+C_2(Z_1,R_1)-2S_1(Z_1,R_1)-C_0(Z_1,R_1)+I_2(Z_1,R_1))$$

$$+\beta_2(1+C_2(Z_2,R_2)-2S_1(Z_2,R_2)-C_0(Z_2,R_2)+I_2(Z_2,R_2))\Big\}$$

$$\div\Big\{\beta_1(I_{-1}(Z_1,R_1)+I_1(Z_1,R_1)-2S_0(Z_1,R_1)-C_{-1}(Z_1,R_1)+C_1(Z_1,R_1))$$

$$+\beta_1(I_{-1}(Z_2,R_2)+I_1(Z_2,R_2)-2S_0(Z_2,R_2)$$

$$-C_{-1}(Z_2,R_2)+C_1(Z_2,R_2))\Big\}\ , \tag{77}$$

where according to Equations 42 – 44 (with the appropriate corrections, i. e. replacing Z and $\overline{a}$ with $Z_{1/2}$ and $\overline{R_{1/2}}$ respectively):

$$I_{-1}(Z_i, R_i) = \frac{Z_i + 1}{q\overline{R_i}Z_i} \ , \tag{78}$$

$$I_1(Z_i, R_i) = q\overline{R_i} \ , \tag{79}$$

$$S_0(Z_i, R_i) = (1 + (\frac{2q\overline{R_i}}{Z_i + 1})^2)^{-\frac{Z_i+1}{2}} \sin\left\{(Z_i + 1)\arctan(\frac{2q\overline{R_i}}{Z_i + 1})\right\} \ , \tag{80}$$

$$C_{-1}(Z_i, R_i) = \frac{Z_i + 1}{q\overline{R_i}Z_i}(1 + (\frac{2q\overline{R_i}}{Z_i + 1})^2)^{-\frac{Z_i}{2}} \cos\left\{Z_i\arctan(\frac{2q\overline{R_i}}{Z_i + 1})\right\} \ , \tag{81}$$

$$C_1(Z_i, R_i) = q\overline{R_i}(1 + (\frac{2q\overline{R_i}}{Z_i + 1})^2)^{-\frac{Z_i+2}{2}} \cos\left\{(Z_i + 2)\arctan(\frac{2q\overline{R_i}}{Z_i + 1})\right\} \ , \tag{82}$$

and $i = 1, 2$. Equations 78 – 82 are of course very similar to Equations 57 – 61. The other integrals not explicitly mentioned here are given as Equations 68 – 72.

Equation 77 can be rewritten in the following form:

$$\frac{D_{eff}(0)}{D_{eff}(q)} =$$

$$(\kappa\frac{\overline{R_1^5}}{\overline{R_2^5}} + 1)/(\kappa q\overline{R_1}\frac{\overline{R_1^5}}{\overline{R_2^5}}\frac{Z_1 + 6}{Z_1 + 1} + q\overline{R_2}\frac{Z_2 + 2}{Z_2 + 1})$$

$$\times\left\{1 + \kappa + \kappa(C_2(Z_1, R_1) - 2S_1(Z_1, R_1) - C_0(Z_1, R_1) + I_2(Z_1, R_1))\right.$$

$$\left. +(C_2(Z_2, R_2) - 2S_1(Z_2, R_2) - C_0(Z_2, R_2) + I_2(Z_2, R_2))\right\}$$

$$\div\left\{\kappa(I_{-1}(Z_1, R_1) + I_1(Z_1, R_1) - 2S_0(Z_1, R_1) - C_{-1}(Z_1, R_1) + C_1(Z_1, R_1))\right.$$

$$+(I_{-1}(Z_2, R_2) + I_1(Z_2, R_2) - 2S_0(Z_2, R_2)$$

$$\left. -C_{-1}(Z_2, R_2) + C_1(Z_2, R_2))\right\} \ , \tag{83}$$

where κ is defined in Equation 75 and the relation

$$\frac{\overline{R_i^6}}{\overline{R_i^5}} = \frac{I_6(Z_i, R_i)}{I_5(Z_i, R_i)} = \frac{q\overline{R_i}}{Z_i + 1}(Z_i + 6)$$

has been used. The ratio $\overline{R_1^5}/\overline{R_2^5}$ can be calculated in terms of the first moments :

$$\frac{\overline{R_1^5}}{\overline{R_2^5}} = \frac{I_5(Z_1, R_1)}{I_5(Z_1, R_1)} = \frac{\overline{R_1}^5}{\overline{R_2}^5}\frac{(Z_1 + 5)(Z_1 + 4)(Z_1 + 3)(Z_1 + 2)}{(Z_2 + 5)(Z_2 + 4)(Z_2 + 3)(Z_2 + 2)}\frac{(Z_2 + 1)^4}{(Z_1 + 1)^4} \ . \tag{84}$$

With this relation Equation 83 was used for fitting to the dynamic scattering data. The parameters $Z_{1/2}$, $R_{1/2}$, κ, and an amplitude were varied until the expected (normalized) apparent size agreed well with the measured values for the (unnormalized) apparent size.

CHAPTER IV

EXPERIMENTS

General Procedure

The objective of this study was the examination of single scattering samples. To ensure that each scattered photon hits only one scattering particle, the concentrations have to be very low. Only minute amounts of particles are necessary to satisfy this condition. Since all particles used came in lots with volume fractions on the order of 10 %, those suspensions had to be diluted with the appropriate solvent. The volume fractions of the final scattering samples were between about 0.01 % for the PMMA and 0.001 % for the polystyrene particles. It is somewhat difficult to measure very small volume fractions exactly due to the small amounts of particles involved. The samples were prepared in cylindrical quartz cuvettes of outer diameter 10 mm and height 700 mm. The cuvette was almost filled with solvent, a drop of the concentrated stock was added with a pipette, and the mixture was shaken severely to get a uniform concentration within the whole cell. A large part of this mixture was then taken out and discarded. The remaining suspension in the cell was diluted again by adding clean solvent. This procedure of tumbling the mixture, taking out part of it and refilling the cuvette with solvent was repeated several times. The desired volume fraction was assumed to be reached when the sample viewed against a bright source of white light seemed almost clear except showing a very dim blue shimmer. If the sample was too concentrated, multiple scattering would contribute to the measurements. If, on the other hand, the concentration was too low, no useful measurements would be possible (especially at high scattering angles) because of the weak signal strength. A teflon stopper protected the cuvette's contents from evaporation and contamination by dust. An extra seal of teflon tape and parafilm in the case of PMMA
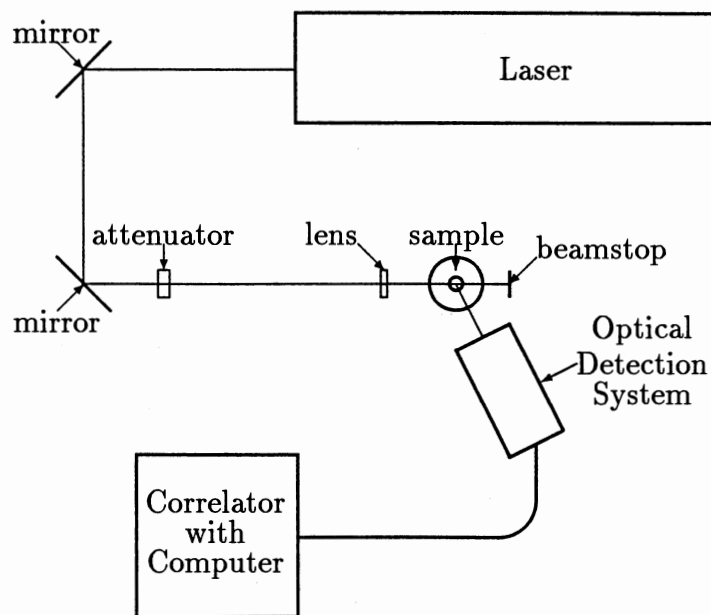
Figure 1. Experimental Setup

particles slowed evaporation. For the samples with water as the solvent, merely parafilm was sufficient. After preparation of a sample and repeated tumbling and shaking of the glass cell, the cuvette was placed into the teflon sample holder of the scattering apparatus. To reduce reflections at the glas-air interface the whole cell was partially submerged in an index matching bath of toluene. The sample was left in this bath for 30 minutes to allow the temperature to equilibrate within the toluene/water system. This was done to limit the effects of convection currents influencing the light scattering measurements. The scattering setup is pictured in Figure 1. A Spectra-Physics Argon ion laser (model 2020) provided the source of light at the green 514.5 nm line. The output of this laser can be regulated between 200 mW and 5 W. However the highest intensities used corresponded to a power output of 1.5 Watts. Since all samples scattered quite strongly into the forward direction the intensity had to be adjusted with a Newport M925B linear attenuator at small scattering angles. The laser light is reflected off two mirrors, directed through the attenuator and focussed into the center of the scattering cuvette. The waist of the beam is about 300 μm wide. A photomultiplier tube is mounted on

a computer controlled goniometer arm in such a way that it is focussing onto the center of the cuvette also. A pinhole with a diameter of 200 μm blocks stray light from entering the phototube. The dead time of that phototube is smaller than 1 nsec thus causing no interference with the measurements (the time scale of which is on the order of microseconds). The output from this tube is sent to a digital multiple tau correlator board that calculates the correlation function of the scattered light in realtime. The equipment described is part of the light scattering package "ALV-5000" purchased from ALV-Laser Company, Germany. The correlator uses the 286 processor of its host computer, an IBM AT personal computer which made storage, data analysis and user input possible. The software package accompanying the "ALV-5000" contains a program generator that allows for runs under automated program control. This feature was used with the samples. Starting at small angles (16 degrees in the case of the PMMA particles) and going to higher scattering angles (up to 140 degrees) the correlation function was measured in half a degree (one degree) steps for the PMMA (for all other samples). Because the form factor (= the angular intensity profile) of the examined particles was not at all constant the whole sweep, from small to large angles could not be done in one run. Several times the run had to be interrupted to adjust the intensity of the laser in such a way that the count rate obtained from the photomultiplier was between 50 KHz and 250 KHz. This adjustment always corresponded to an increase in laser intensity either by decreasing the attenuation or by increasing the power of the laser itself. The duration of each measurement of the correlation function was 1000 seconds — ensuring sufficient statistical accuracy by taking data over a period of 10^6 decay times of the correlation function. Thus some of these runs extended over several days, and it was necessary to interrupt a run to redisperse the particles, making sure that settling out of the measurement volume would not interfere with the experimental success. This was only necessary for the PMMA in organic solvents, since those settled during the experiment due to their size, the ratio of particle/solvent density, and the extremely long duration of a complete run. The other particles settled more slowly and no redispersing was needed. The

correlation function from each scattering angle was stored on disc together with the average intensity of the run at the particular angle. (The feasability of simultaneous static and dynamic light scattering data was reported by Bantle, Schmidt, and Burchard [41].) The software of the "ALV-5000" supports an immediate cumulant analysis of the correlation function after the measurement. This utility was used and the result accompanied by the scattered intensity written into an ASCII log file. These log files provide a fairly detailed description of the whole run and are very efficiently used for further data analysis. A DOS batch file extracted the necessary information out of these files and transformed them into spreadsheet readable format. Most of the data analysis was performed after importing those stripped files into the Borland spreadsheet program Quattro Pro. The following sections describe the individual compositions of the samples used.

PMMA in Organic Solvents

The stock bottle of polymethylmethacrylate (PMMA) contained spheres of radius 495 nm with a standard deviation of less than 5 % . These particles are sterically stabilized with a layer of poly-12-hydroxystearic acid (about 10 nm layerthickness) to prevent aggregation caused by Van-der-Waals attraction [42]. The initial stock was in the solvent dodecane ($C_{12}H_{26}$). It was 'washed' with decalin (Decahydronaphtalene, $C_{10}H_{18}$). The solvent exchange procedure consisted of tumbling the bottle with solvent, centrifuging, decanting the supernatent, exchanging with the new solvent and redispersing again. This procedure was repeated six times. An estimate of the contamination with the original solvent dodecane is $((\frac{1}{3})/(\frac{3}{2}))^7 = (\frac{2}{9})^7 = 0.003$ % ; one third being the fraction of solvent in the centrifuged sediment and $\frac{3}{2}$ being the new total volume after adding the new solvent. The cleaned stock provided the particles for the preparation of three PMMA samples. Since the concentration after the washing was about 30 %, a small amount of stock was needed. One drop of this stock was pipetted into a sample cell containing pure decalin. This was repeated with a sample cell containing pure tetralin (1,2,3,4-Tetrahydronaphtalene, $C_{10}H_{12}$) and another cell containing a mixture of

decalin and tetralin. This mixture had an index of refraction of 1.51, thus closely matching the refractive index of the particles. The volume fractions of decalin and tetralin required for this index match have been determined in an earlier study on crystallization of PMMA reported by Paulin and Ackerson [43]. A fourth sample of these PMMA spheres was obtained using carbon disulfide (CS_2) as the solvent. As mentioned in the General Procedure section of this chapter, the run over all angles started immediately after preparing the sample and a short temperature equilibration wait. The angle increments were 0.5 degrees. Because of the size of the scattering objects, the intensity dropped over 4 orders of magnitude over the range of angles examined. This fact required the division into 5 subruns with readjusting the count rate in between those subruns. The samples 'PMMA in Decalin' and 'PMMA in Tetralin' were measured between 16 and 140 degrees. The samples 'PMMA in Decalin/Tetralin Mix' and 'PMMA in Carbon Disulfide' were measured from 16 to 120 degrees in the 0.5-degree-steps.

PMMA in Water

A totally different sample of PMMA spheres was also used. This sample was obtained from DOW Chemicals. These PMMA were quoted to have a radius of 325 nm. They had a different unknown coating which was hydrophilic and allowed dispersion in water. Again a drop from the stock bottle was the foundation of the sample prepared in a cuvette with clean water as the solvent. This sample was measured from 40 degrees to 75 degrees in 1 degree steps.

TPM-silca in Ethanol

The particles consist of a core of Silica that is coated with 3-(trimethoxysilyl)propyl methacrylate (TPM). The TPM-chains function as a steric stabilizer like the poly-12-hydroxystearic acid chains on the PMMA particles. TPM-silica can be index matched with a mixture of toluene ($C_6H_5CH_3$) and ethanol (CH_3CH_2OH). In this study the particles were examined using pure ethanol as

the solvent. However a small contamination took place because the stock bottle contained some toluene. These particles were developed only recently as a model system for studies of colloidal properties. They are spherical and have a nominal radius of 250 nm. This sample was measured from 40 degrees to 90 degrees in 1 degree steps.

PST in Water

Particles made out of polystyrene (PST) are well established in light scattering. They are easily commercially available and widely used. The linear PST molecules are crosslinked in such a way that many hydrophilic groups at the ends of the chains reside on the surface of the particle [6]. In a polar solvent, those surface groups ionize and cause the particle to be negatively charged. The stabilization is thus called charge stabilization — the particles are protected against aggregation by their like charge. The samples used contained spheres with radii of 250 nm, 300 nm and 500 nm. The particles were dispersed in clean water. The standard deviation of the radii is less than 5 % . For the sample labelled "PST 500" the correlation function and the scattered intensity were measured from 20 degress to 75 degrees in 1 degree steps. The sample labelled "PST 600" contained recently prepared polystyrene spheres with a standard deviation less than 3 % . This sample was measured from 30 to 90 degrees in 1 degree steps. An additional sample containing these "PST 600" particles was intentionally contaminated with a known number of PST spheres of radius 500 nm which had a standard deviation less than 5 %. For this sample labelled "PST 600/1000", data were taken between 30 degrees and 120 degrees in 1 degree steps.

Tests and Additional Experiments

Several tests and experiments preceded those reported in the previous sections of this chapter. This series of experiments started with taking dynamic and static scattering data on PMMA samples in the solvents decalin, tetralin and a

mixture of the two. Those were similar to the runs described in the section 'PMMA in Organic Solvents' of this chapter. The angular resolution was not as fine (5 degree steps instead of half degree steps) and the duration of each run was 3 minutes. Since the data appeared to show some "inconsistencies"— namely the apparent size seemed to be larger at the minima of the form factor and the positions of those minima of the PMMA in tetralin sample did not fit Rayleigh-Debye-Gans theory — a new set of samples was prepared. The particles used for this group came from a different batch of PMMA. Those particles were supposed to have about the same radius, but were produced separately from the first batch. Again three samples of PMMA (decalin, tetralin, decalin/tetralin mix) were prepared. But even with these samples, the dynamic scattering was not constant over all angles (which would be expected for a perfect sample). The intensity showed the same disposition of the minima for the tetralin case. The form factor minima of PMMA in decalin and PMMA in tetralin were again at almost the same angles. This implied that the PMMA particles in tetralin were *smaller* than the PMMA in decalin (because $n_{tetralin} > n_{decalin}$). This seemed to be in contradiction to the trend observed with the dynamic light scattering: the particles in tetralin had (on average) a larger radius than the ones in decalin. Since a third batch of PMMA particles was available, three more samples were prepared. But the static light scattering of these still exhibited the strange behavior for the tetralin case. The results pointed towards tetralin penetrating into the particles. Fitting the intensity data to a core/shell model instead of the RDG uniform sphere model produced a somewhat better result. Under this assumption, the particle has a core surrounded by a shell with a different index of refraction. This model made the explanation of the smaller static radius possible by assuming that the tetralin penetrated the outer regions of the PMMA. If this shell has a refractive index very close to tetralin, the contrast between the shell and the solvent can be smaller than the contrast between the core and the shell. Thus the higher contrast scattering is dominant and makes an effectively smaller size obtained from the static data possible. However the dynamic data could still not be explained: at the maxima of the form factor

the dynamic scattering was consistent, but at the minima the radius from the fit to the correlation function was always 'wrong', i. e. too big.

Dust was then suspected to cause the trouble: at those form factor minima angles, almost no intensity comes from the particles and 'anything else that scatters' can enter into the measurement. The static scattering of the pure solvents (as they were used to prepare the samples) was compared to the scattering of destilled toluene ($C_6H_5CH_3$) which is often used as a standard. The absolute intensities of the four solvents were different but showed the same functional dependence on the scattering angle ($\sin(\theta)$-law, the scattered intensity is proportional to the scattering volume which in turn is proportional to the sine of the scattering angle). Thus there was no dust in the solvents. To investigate if the stock particles were contaminated by dust or large aggregates, a PMMA in decalin sample was shaken up, measured on the same day and measured again two days later. But the dynamic scattering continued to show the upswing in the apparent size when the scattering intensity was close to a minimum. Evidently there were no large aggregates to settle out. However a sample of polystyrene in water that was run later gave a good example of results in the presence of contamination of the solvent and/or the particles. The apparent size from the correlation function measurements had several big jumps in it, and these jumps occured even at angles where the form factor was close to a maximum where enough scattering from the main particles is expected. After filtering that sample, these jumps disappeared.

In another set of experiments, the effects of concentration were examined. Samples more concentrated than the previous ones (approximately by a factor of 5) were prepared and measured. The scattering of these samples was still single scattering, but they definitely scattered more intensely. Nevertheless the dynamic data were still not good at the form factor minima. These samples were also watched over a period of several weeks. If tetralin was penetrating the outer regions of the PMMA, then this should appear in the static scattering as a change over time. The core radius decreased slightly but not significantly. Another observation was the irregular pattern of the static scattering of the PMMA in the decalin/tetralin

mixture. The form factor of these samples changed somewhat randomly within certain limits. But the static scattering from all samples near index match could never be explained in a satisfactory way.

The form factor minima were never as deep as predicted by both RDG and the core/shell theory. This might be due to background scattering caused by irregularities in the wall of the scattering cell. But a measurement of a PMMA in decalin sample in a quartz cell and in a glass cell did not support this hypothesis. The static scattering with the quartz cell was the same as the static scattering with the glass cell. (The minima in the glass cell were slightly deeper but not at all enough to lie on the theory curve.)

Was multiple scattering causing the problem? Multiple scattering is present if light gets scattered by two or more particles before entering the optical detection system. This causes the correlation function to decay *faster* due to the Brownian motion of two or more particles involved now. It takes less time for the combination of particles to move one wavelength than it takes for just one particle. This is equivalent to a faster decay of the correlation function and thus a smaller size — as opposed to the larger size observed at certain angles. Multiple scattering also changes the polarization of the incident radiation. Examining samples illuminated by the polarized laser showed clearly that there was almost no intensity in the crossed position, that is if the detected polarization was perpendicular to the polarization of the light emitted by the laser. There was a small fraction ($\stackrel{<}{\approx} 0.5\%$) of the total intensity scattered into the crossed polarization, but this seemed to be due to the depolarized solvent scattering and not due to scattering by the PMMA particles. To support the examination by eye, one sample, PMMA in decalin, was measured two times with a polarizer in front of the optical detection system. The run with the polarizer in the same orientation as the incident electric field vector showed the usual behavior for both the static and the dynamic scattering. The run with the orientation of the polarizer perpendicular to the incident polarization was harder to measure. The correlation functions measured with this setup were too noisy because of the low count rates of the photomultiplier tube.

There were simply not enough photons arriving at the detector to produce good correlation functions. The intensity was very low. For the lowest angles measured, the static scattering showed the same behavior as the static scattering from the parallel-polarizer-run but then 'drowned' into the background of the solvent. This observation was unexpected. It can have several causes: The polarizer used for these two runs was a cheap polaroid plastic polarizer. (The 0.5% are pretty impressive for the linear polymer plates.) Thus it is not perfect and some radiation with the 'wrong' polarization might pass through. Another possibility is a tilt in the polarization either of the laser or of the molecules in the polarizer. The tilt angle corresponding to an error of 0.5% is less than half a degree.

If the particles where ellipsoidal, a strange behavior in the apparent size could be expected. A major to minor axis ratio of 1.5 would possibly explain the big contributions at the low intensity angles. There are however three arguments against this approach: 1. PMMA do not show any nonsphericity under a microscope. 2. Ellipsoidal particles have a different form factor, the scattered intensity can not be described by the form factor of a sphere (which seems to work well for PMMA in decalin). 3. Considerably more depolarization, than observed, should occur.

In addition to the repeated measurements on different samples, some constants used in the calculation of the apparent size were checked. The indices of refraction of decalin, tetralin and the mixture proved to be 1.48, 1.54 and 1.51 as given in the literature and found in earlier experiments. It is interesting to note at this point that Pusey and van Megen report an index of refration of 1.49 for the PMMA particles whereas here 1.51 is used. Their value for the refractive index was obtained by index matching a sample of PMMA in a mixture of decalin and carbon disulfide. The viscosity of tetralin was also remeasured but found to be the same as the one used in calculating the apparent sizes.

In the attempt to fit the dynamic scattering data, several trial models were tried but rejected. The first try was a monodisperse distribution of particles which produces just a constant line for the apparent size. It should not matter at which

angle the size of the scattering particles is measured by correlation spectroscopy if the particles are uniform.

The Schulz distribution was the next try. Allowing some particles to have a radius smaller or larger than the average changes the apparent size. It does however not fit the data obtained. A main problem is to get considerable contributions from slower decays or larger particles into the correlation function. This can not be done with a core/shell model since the 'viscous-drag-size' does not change with solvent penetrating into the outer layer of the particles (particularly not by a factor of 1.5). A model assuming a few larger particles added to a monodisperse distribution of small (right size) particles could not explain the scattering data very well either. Could the particles stick together and give slower diffusion contributions ? They could, but the form factor corresponding to doublets of spheres is very similar to the form factor of (single) spheres. (A multiplicative function changes only the amplitudes maintaining the minima.) Thus when the scattering of these doublets is needed most, that is at the minima of the (single) sphere form factor, it is small and can not explain the favoring of bigger sizes in the dynamic scattering.

The final model that seems to explain the scattering results best is a combination of two Schulz distributions. This model is used in the following chapter to fit the scattering data from all samples described in the previous sections.

CHAPTER V

RESULTS AND DISCUSSION

Results

The results of the measurements described in chapter VI are presented here. The figures show the experimental data and the best fit to those. All fits in the figures are obtained using Equation 74 for the intensity data and Equation 83 for the dynamic light scattering results. Thus the 'theoretical' lines in the plots imply a particle size distribution that can be described by two Schulz distributions (see Equation 62). The parameters of this double Schulz distribution are κ (Equation 75), the two average radii $R_{1/2}$, and the two corresponding polydispersity indicators $Z_{1/2}$. The values of the parameters chosen for the best fit are given in the figure captions of the corresponding display of the experimental results. The best fit was obtained "by eye" and involved a series of different trial parameters.

PMMA in Decalin

The form factor of the PMMA spheres in decalin is shown in Figure 2. The fit with Equation 74 matches well in the center part of the angular range. However the agreement at small and large angles is not as good. This might be due to dust or aggregates at small scattering angles and due to internal reflections in the scattering apparatus/cell at large angles [41]. The results of the cumulantfit to the autocorrelation function are shown in Figure 3. The maxima in the apparent size occur at those scattering angles where the form factor has a minimum. The fit implies that a vast majority of the particles have the expected radius, ≈ 500 nm . There is however a small contribution (around 0.5 %) of bigger particles in the solution. The polydispersity of these big 'chunks' is very large: $\sigma = 41$ %. The
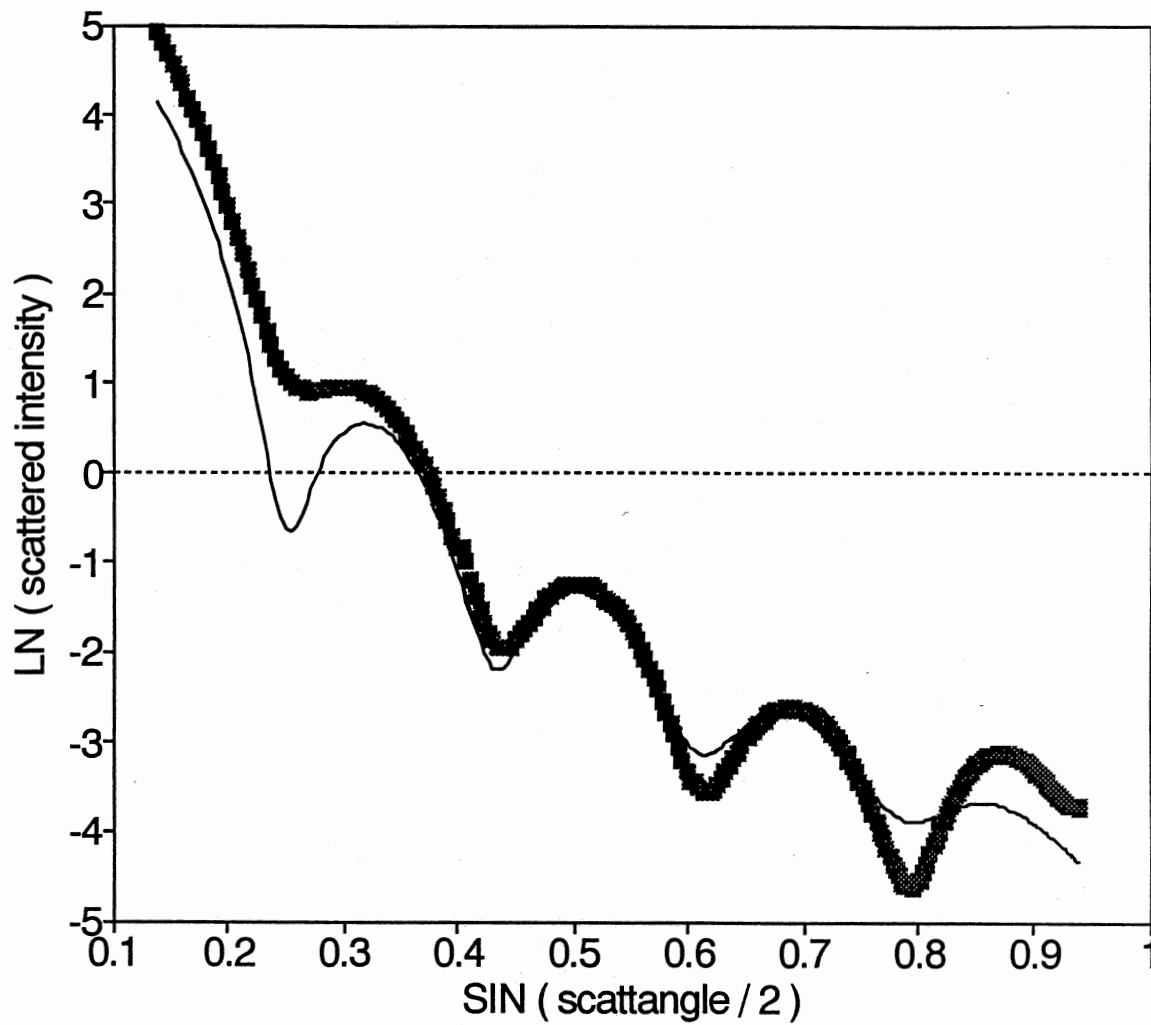
Figure 2. Form Factor of PMMA in Decalin. The natural logarithm of the scattered intensity is plotted versus $\sin(\theta/2)$. The fit (solid line) is calculated using $\overline{R_1} = 495$ nm, $\overline{R_2} = 2000$ nm, $\kappa = 200$, $Z_1 = 350$, and $Z_2 = 5$.
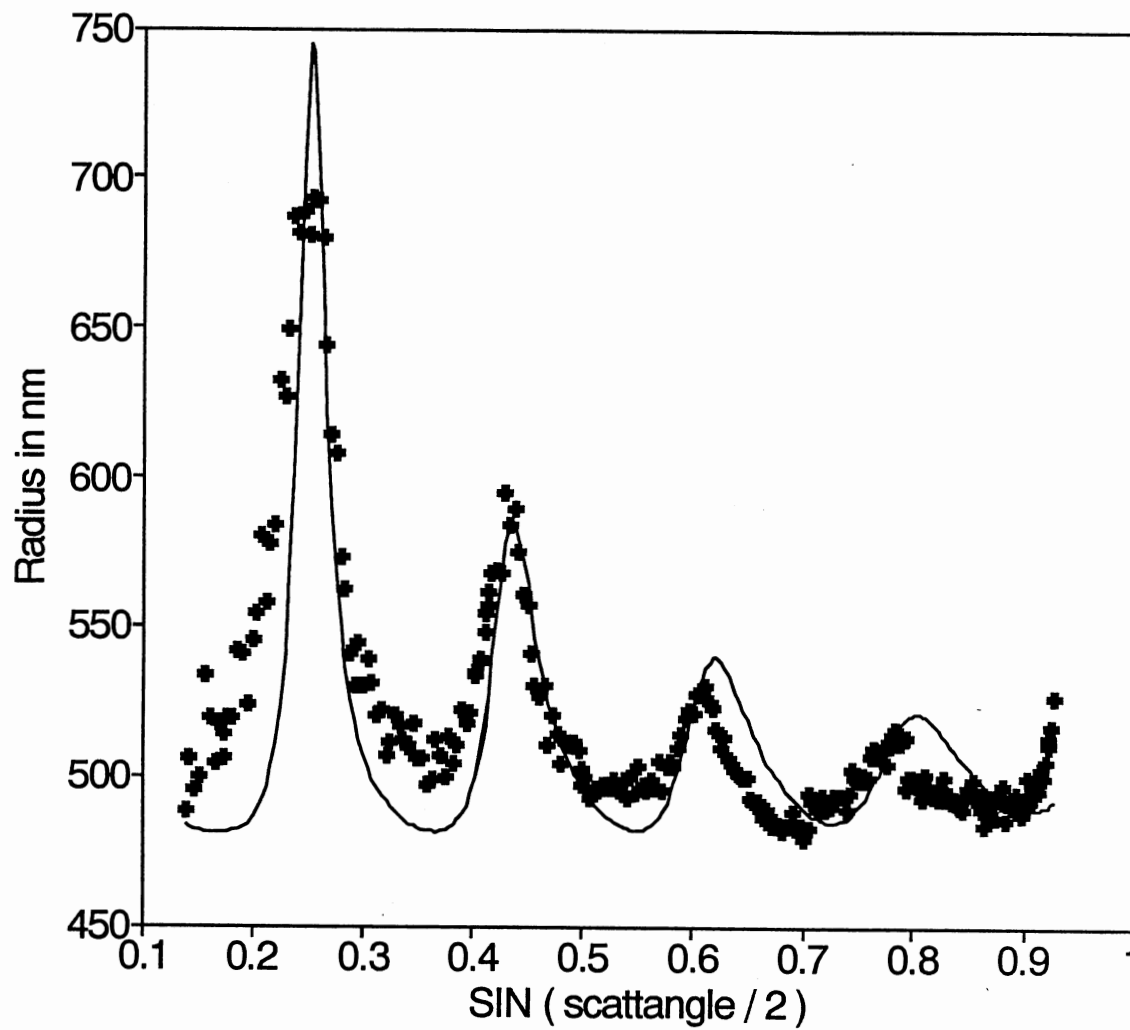
Figure 3. Dynamic Radius versus $\sin(\theta/2)$ of PMMA in Decalin. The fit (solid line) is calculated using $\overline{R_1} = 495$ nm, $\overline{R_2} = 2000$ nm, $\kappa = 200$, $Z_1 = 350$, and $Z_2 = 5$.

polydispersity of the main species is 5 %. This agrees with reports of crystallization by Paulin and Ackerson [43], where particles were not expected to crystallize had their polydispersity been larger than about 7 % [6]. The maxima in the apparent size occur at those scattering angles where the form factor of the main particles has a minimum. Only at these angles can the big particles contribute noticeably to the correlation function. This can also be seen from the signal to noise ratio in Figure 4. There is more noise at the form factor minima than at the other scattering angles. The decrease of the signal to noise ratio can however not be attributed entirely to the big particles. Another unmentioned scource of noise at the intensity minima is the background and the solvent scattering. Figure 5 shows a plot of the particle size distribution according to Equation 62 with the values found by fitting the static and the dynamic scattering data.

PMMA in Tetralin

The form factor of the PMMA spheres in tetralin is shown in Figure 6. The measured minima are not as deep as they should be according to the fit. This might be due to the solvent scattering — the background scattering that was not subtracted. The positions of the minima agree with the 'theory' very well, though. The apparent size from the cumulant fit to the correlation function is plotted in Figure 7. The pronounced maxima of the dynamic radius occur at the form factor minma angles. This is very similar to the behavior observed with the same particles in decalin (see Figure 3). The fit suggests a majority of the particles have a radius of ≈ 470 nm . A 'contamination' (around 0.5 %) of bigger particles (1700nm) is needed to obtain a good fit. The polydispersity of these big 'chunks' is — as with PMMA in decalin — large: $\sigma = 30$ %. The polydispersity of the main species is 5 %. The maxima in the apparent size occur at those scattering angles where the form factor of the main particles has a minimum. The positions of those form factor minima are unfortunately not exactly where they should be: the minima occur at scattering angles that are slightly too large. This results in the smaller size of the main species. An explanation of this behavior might be the influence of
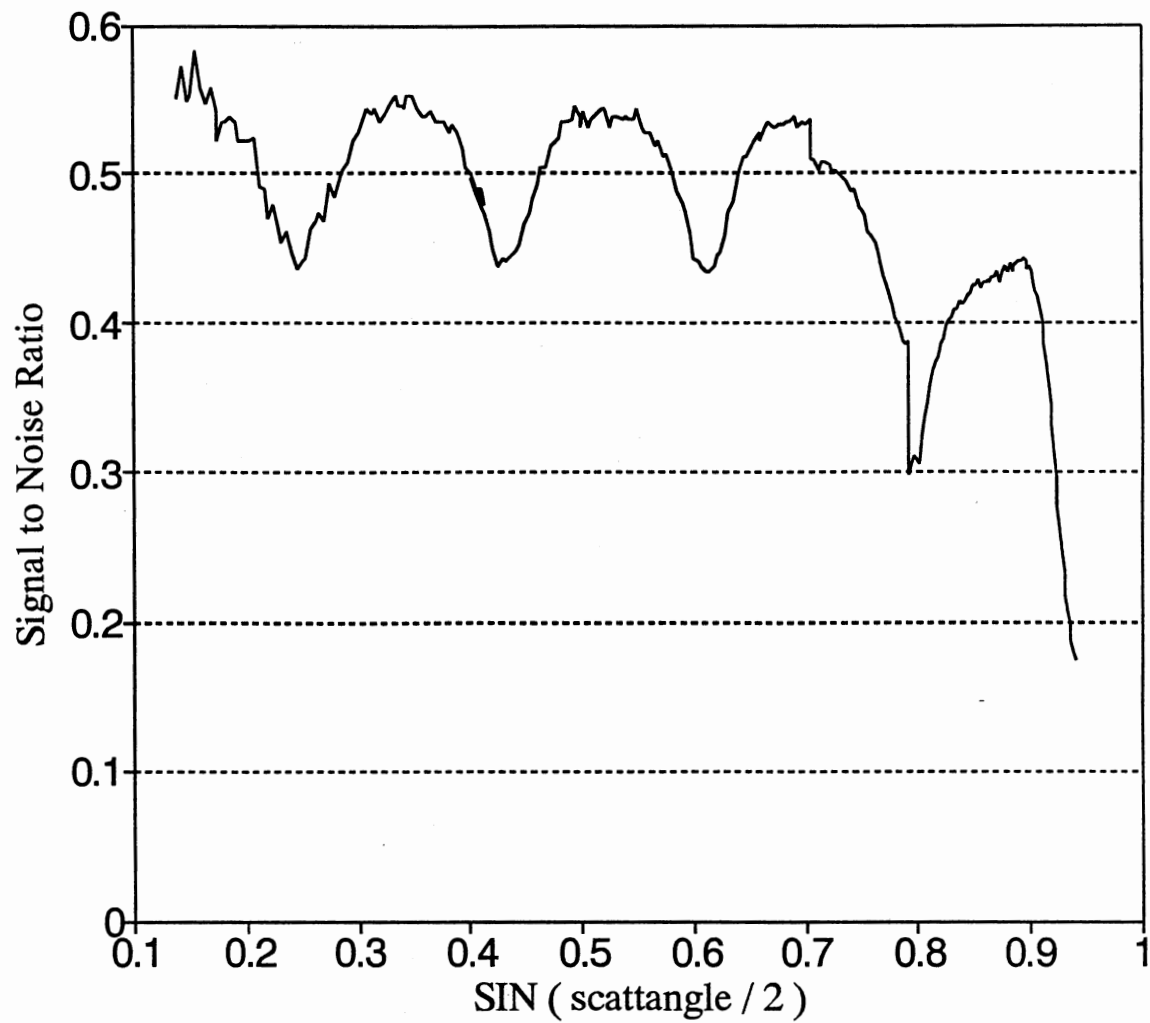
Figure 4. Signal to Noise Ratio of PMMA in Decalin. The intercepts of the measured intensity correlation functions are plotted versus $\sin(\theta/2)$.
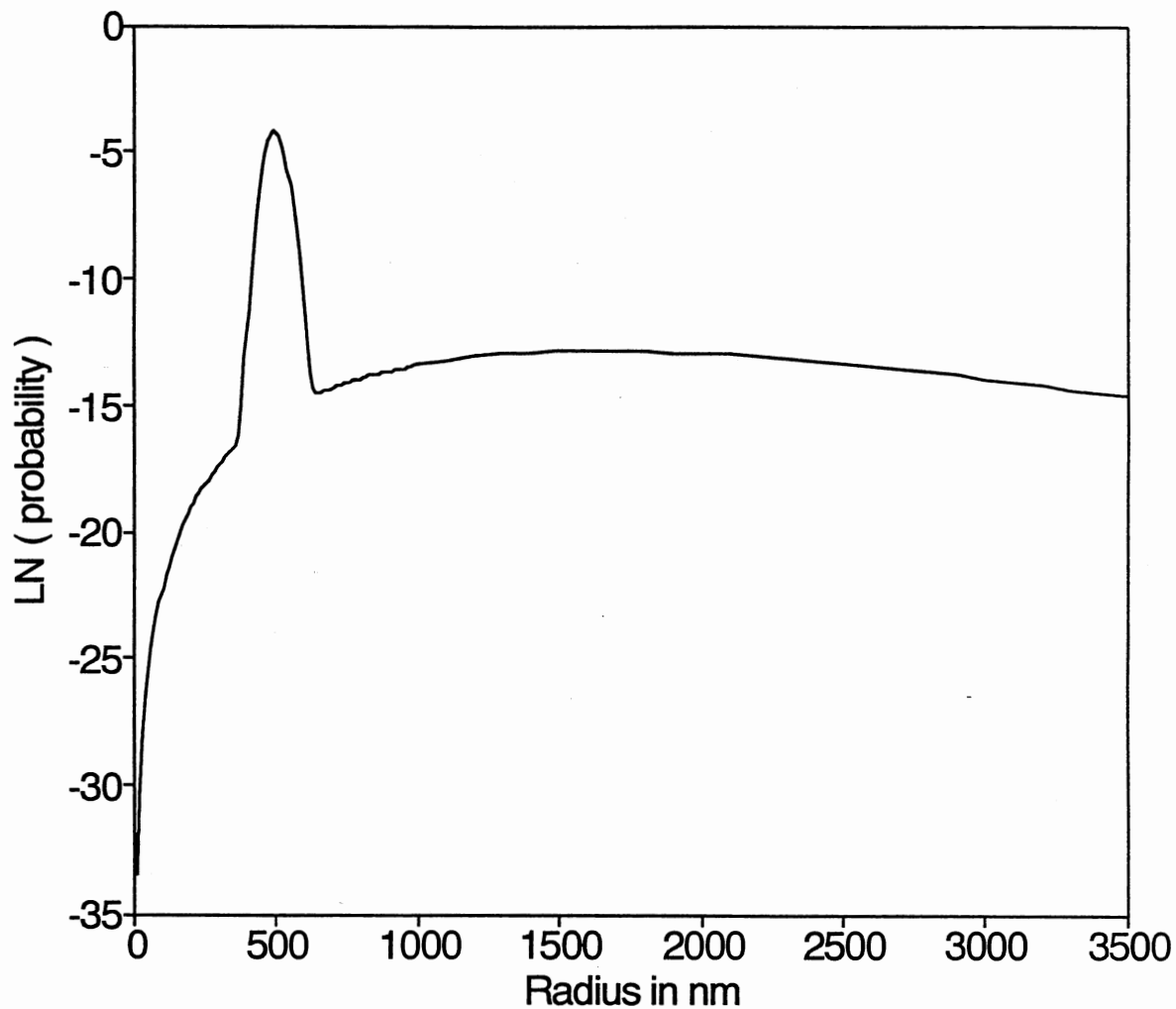
Figure 5. Particle Size Distribution of PMMA in Decalin. The plot shows the natural log of the normalized probability of finding a particle versus the radius of that particle in nm. The distribution is calculated using $R_1 = 495$ nm, $R_2 = 2000$ nm, $\kappa = 200$, $Z_1 = 350$, and $Z_2 = 5$.
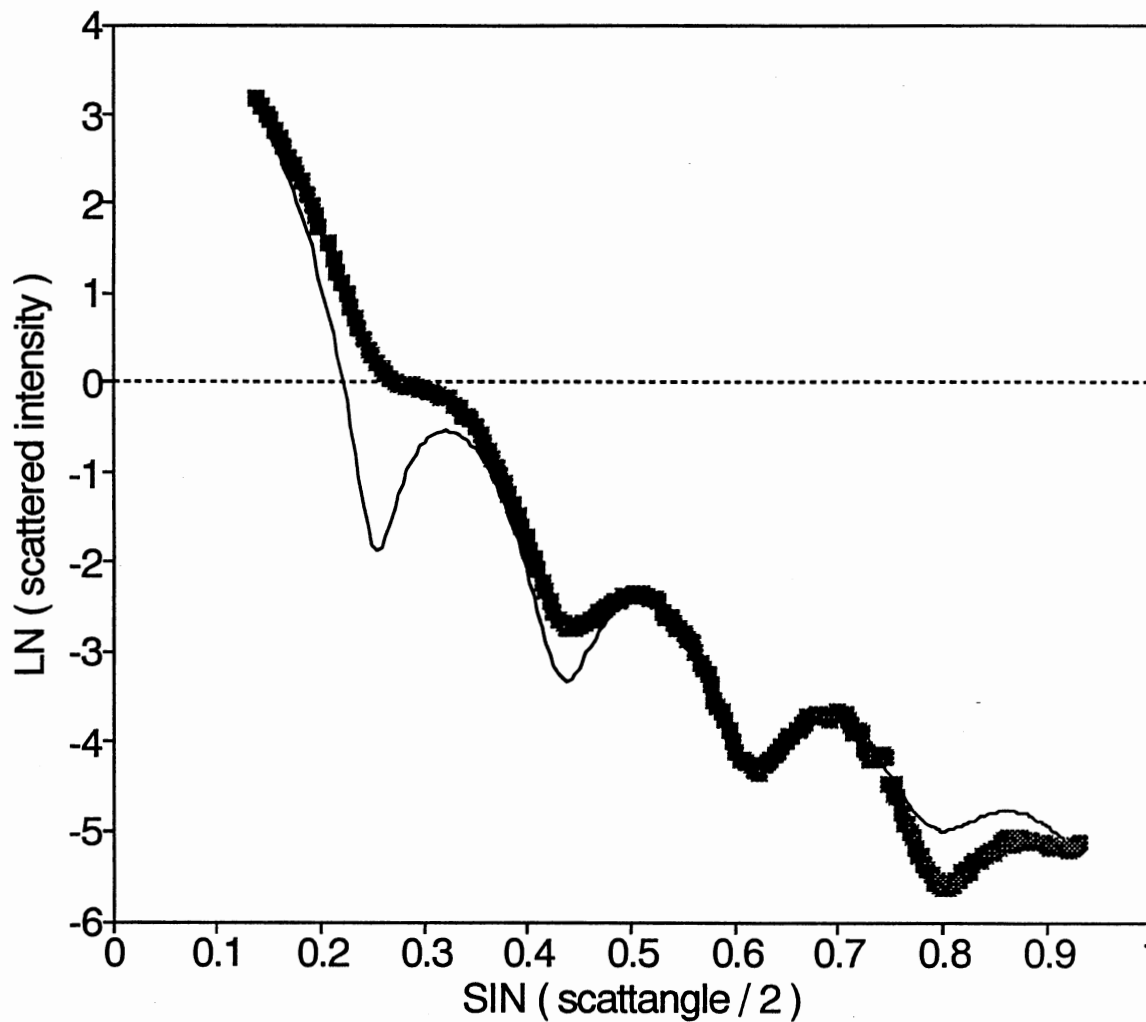
Figure 6. Form Factor of PMMA in Tetralin. The natural logarithm of the scattered intensity is plotted versus $\sin(\theta/2)$. The fit (solid line) is calculated using $\overline{R_1} = 470$ nm, $\overline{R_2} = 1700$ nm, $\kappa = 200$, $Z_1 = 350$, and $Z_2 = 10$.
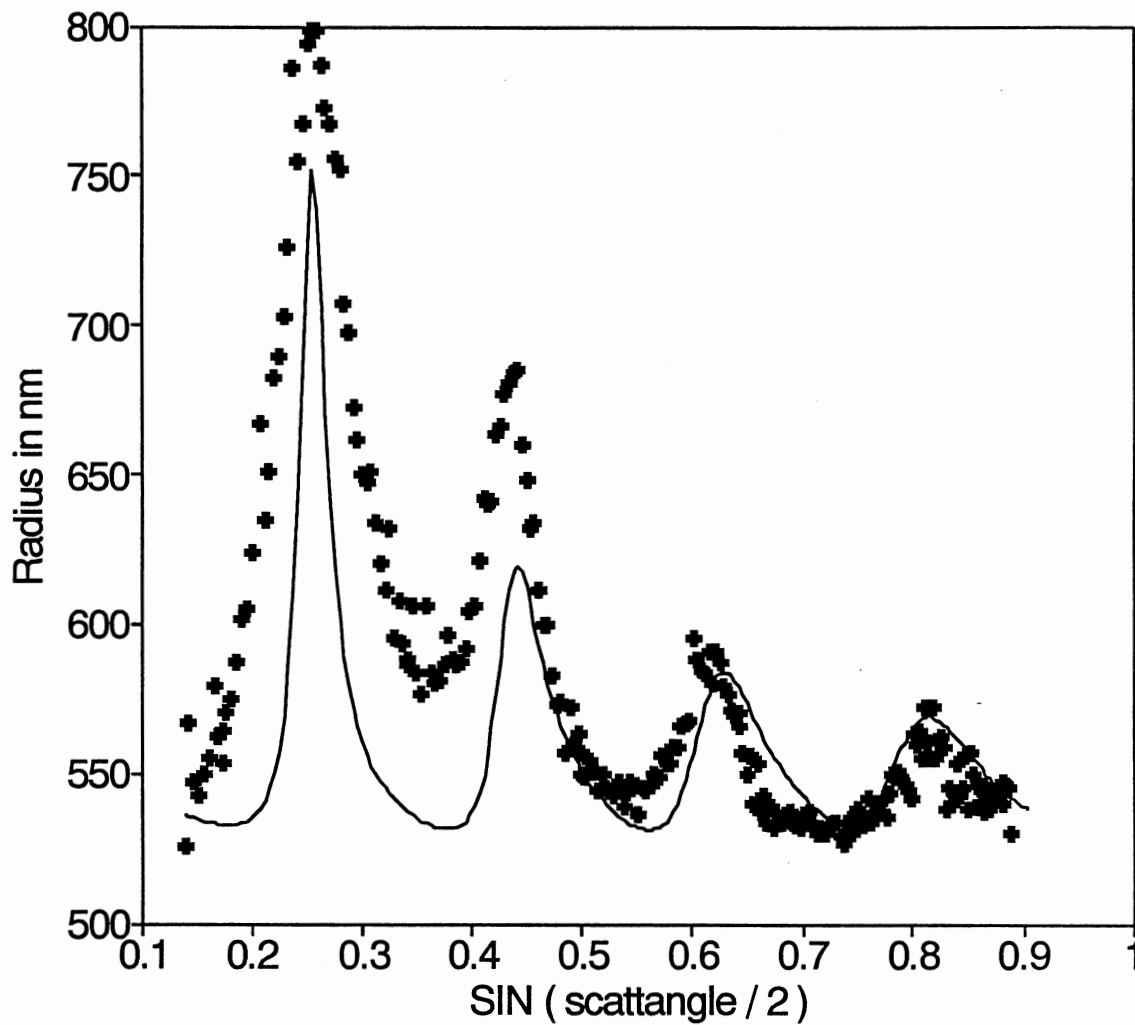
Figure 7. Dynamic Radius versus $\sin(\theta/2)$ of PMMA in Tetralin. The fit (solid line) is calculated using $\overline{R_1} = 470$ nm, $\overline{R_2} = 1700$ nm, $\kappa = 200$, $Z_1 = 350$, and $Z_2 = 10$.

a shell around the particle [44] or more exactly tetralin penetrating into the outer regions of the sphere. That would cause the size 'seen' by static light scattering to be smaller than the original size without solvent penetrating through the surface of the spheres.

PMMA in Decalin/Tetralin Mixture

The form factor of the PMMA particles suspended in a mixture of decalin and tetralin is shown in Figure 8. The values for the parameters $\overline{R_{1/2}}$, $Z_{1/2}$, and κ are obtained from the fit to the dynamic scattering data of Figure 9. This sample presents problems because the index of the particles is very close to the index of the surrounding solvent. This causes 'strange' effects: slight variations in the indices of refraction — for example due to temperature fluctuations — paired with the additional problem of a core/shell theory produce an angular intensity profile that is hard to explain. It is not expected that Equation 74 could be applied in this case. Although the static scattering looks very different from the static results of PMMA in decalin (Figure 2) and from PMMA in tetralin (Figure 6), the dynamic scattering of this sample on the other hand does show similarities to the results of PMMA in decalin (Figure 3) and in tetralin (Figure 7). A low scattering intensity is the reason for the 'cloud' of data points to the right of the first maximum in Figure 9. The count rates at those angles were comparatively low. The cluster of data points between $\sin(\theta/2) = 0.8$ and $\sin(\theta/2) = 0.9$ was measured out of sequence because of a computer problem.

PMMA in Carbon Disulfide

Figure 10 shows the form factor of PMMA suspended in carbon disulfide. The minima of this sample are the least pronounced of all PMMA samples. It contained roughly the same number of particles as the other samples. The solvent scattering was definitely higher than that of the other solvents. After adding particles to the solvent, the whole sample changed from clear to transparent with a milky touch. This clouding effect did not seem to be caused by the particles
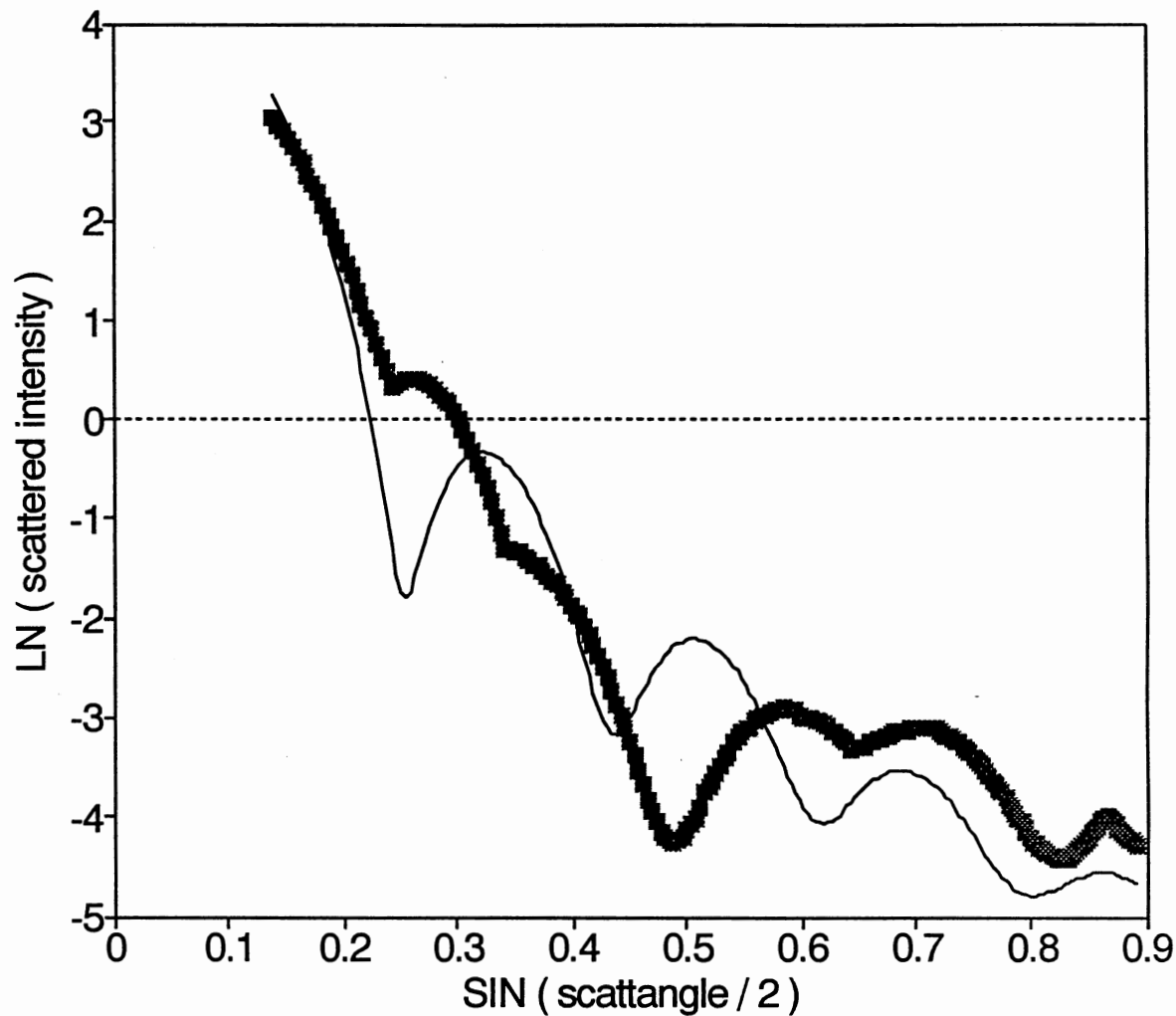
Figure 8. Form Factor of PMMA in Decalin/Tetralin Mix. The natural logarithm
of the scattered intensity is plotted versus $\sin(\theta/2)$. The fit (solid
line) is calculated using $\overline{R_1} = 480$ nm, $\overline{R_2} = 1400$ nm, $\kappa = 200$,
$Z_1 = 350$, and $Z_2 = 10$.

Figure 9. Dynamic Radius versus $\sin(\theta/2)$ of PMMA in Decalin/Tetralin Mix. The fit (solid line) is calculated using $\overline{R_1} = 480$ nm, $\overline{R_2} = 1400$ nm, $\kappa = 200$, $Z_1 = 350$, and $Z_2 = 10$.

Figure 10. Form Factor of PMMA in Carbon Disulfide. The natural logarithm of the scattered intensity is plotted versus $\sin(\theta/2)$. The fit (solid line) is calculated using $\overline{R_1} = 485$ nm, $\overline{R_2} = 3000$ nm, $\kappa = 200$, $Z_1 = 350$, and $Z_2 = 5$.
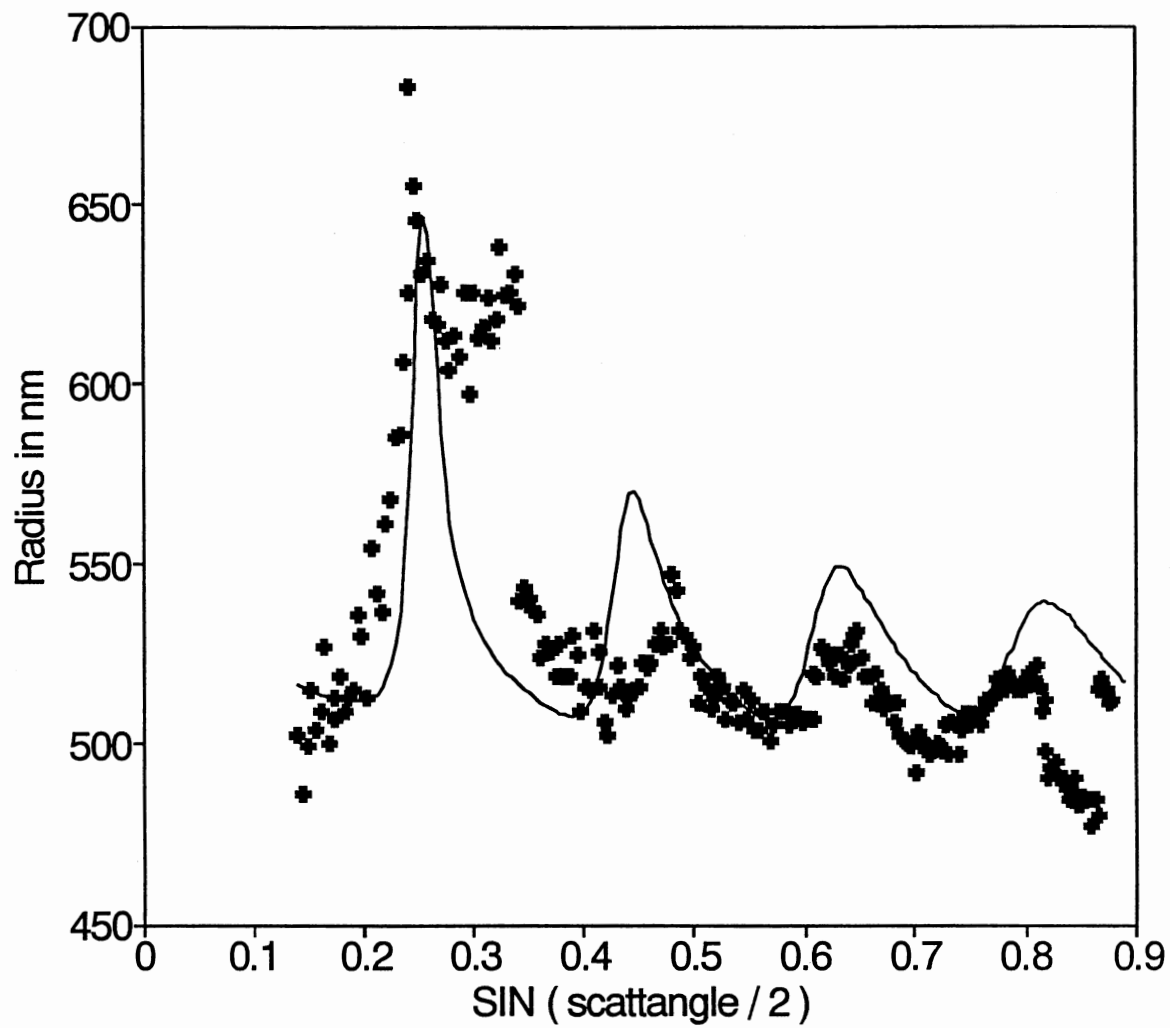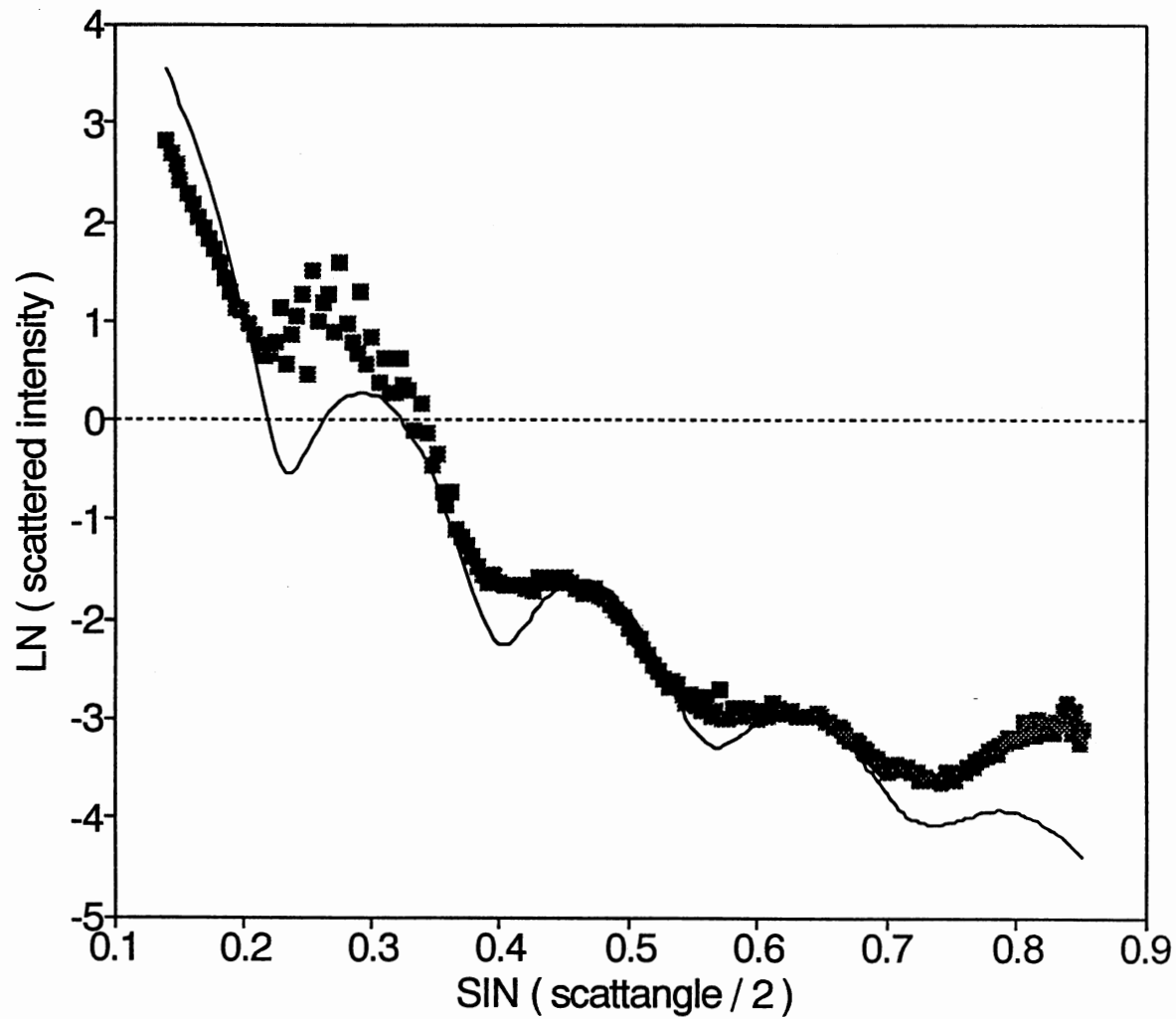
because further dilution did not change the correlation function measured at 60, 90, and 120 degrees; i. e. multiple scattering was not the problem. This favors the argument of an interaction of carbon disulfide with the decalin that was introduced into the sample with the preparation. On the other hand, Pusey and van Megen have successfully used mixtures of decalin and CS_2 in crystallization studies of PMMA [45]. This clouding might be the main reason for the shallowness of the minima in Figure 10. The size of the main species is slightly lower than expected, possibly due to penetration by CS_2 that has been reported by Ottewill and Livsey [46]. The dynamic scattering data show better agreement between the modified Schulz distribution and the apparent size obtained from the cumulant fit of the intensity correlation function: Figure 11 deviates only between the first and the second maximum from the plotted model. The upswing of the measured size at the largest scattering angles is very likely caused by back scattering from the sample cell. The intercept of the correlation functions at these angles was below 0.1, indicating a higher noise content.

PMMA in Water

All previous PMMA samples showed maxima of the apparent size at those angles where the form factor had minima. Since all previous samples contained particles from the same stock bottle, one might suspect that the stock bottle was contaminated with bigger particles. Figure 12 shows the scattered intensity of an entirely different stock of PMMA. The minimum displayed is the first minimum of the sample. The form factor can be fit to several parameter combinations. Here again the dynamic scattering results of Figure 13 influenced the decision towards the chosen set. As with the PMMA in organic solvents, the combination of one main species of particles with a few bigger but very polydisperse particles added produces the best fit. The radius distribution function of this sample is plotted in Figure 14 and shows the same characteristic as Figure 5 : a relatively thin but high peak of small spheres foots on a wide but extremely small mountain of mostly bigger particles.

Figure 11. Dynamic Radius versus $\sin(\theta/2)$ of PMMA in Carbon Disulfide. The fit (solid line) is calculated using $\overline{R_1} = 485$ nm, $\overline{R_2} = 3000$ nm, $\kappa = 200$, $Z_1 = 350$, and $Z_2 = 5$.

Figure 12. Form Factor of PMMA in Water. The natural logarithm of the scattered intensity is plotted versus $\sin(\theta/2)$. The fit (solid line) is calculated using $\overline{R_1} = 360$ nm, $\overline{R_2} = 800$ nm, $\kappa = 200$, $Z_1 = 350$, and $Z_2 = 1$.
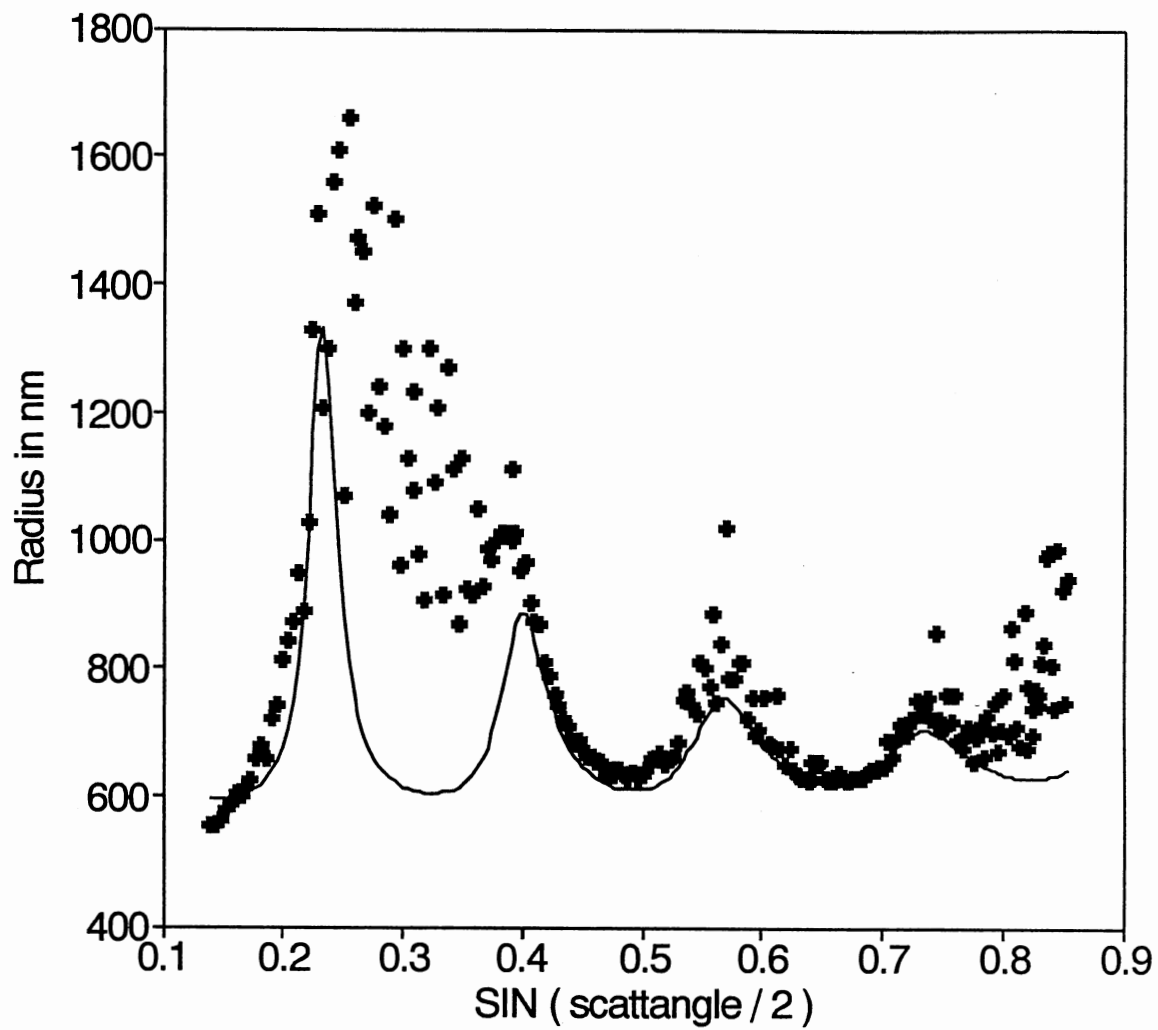
Figure 13. Dynamic Radius versus $\sin(\theta/2)$ of PMMA in Water. The fit (solid line) is calculated using $\overline{R_1} = 360$ nm, $\overline{R_2} = 800$ nm, $\kappa = 200$, $Z_1 = 350$, and $Z_2 = 1$.
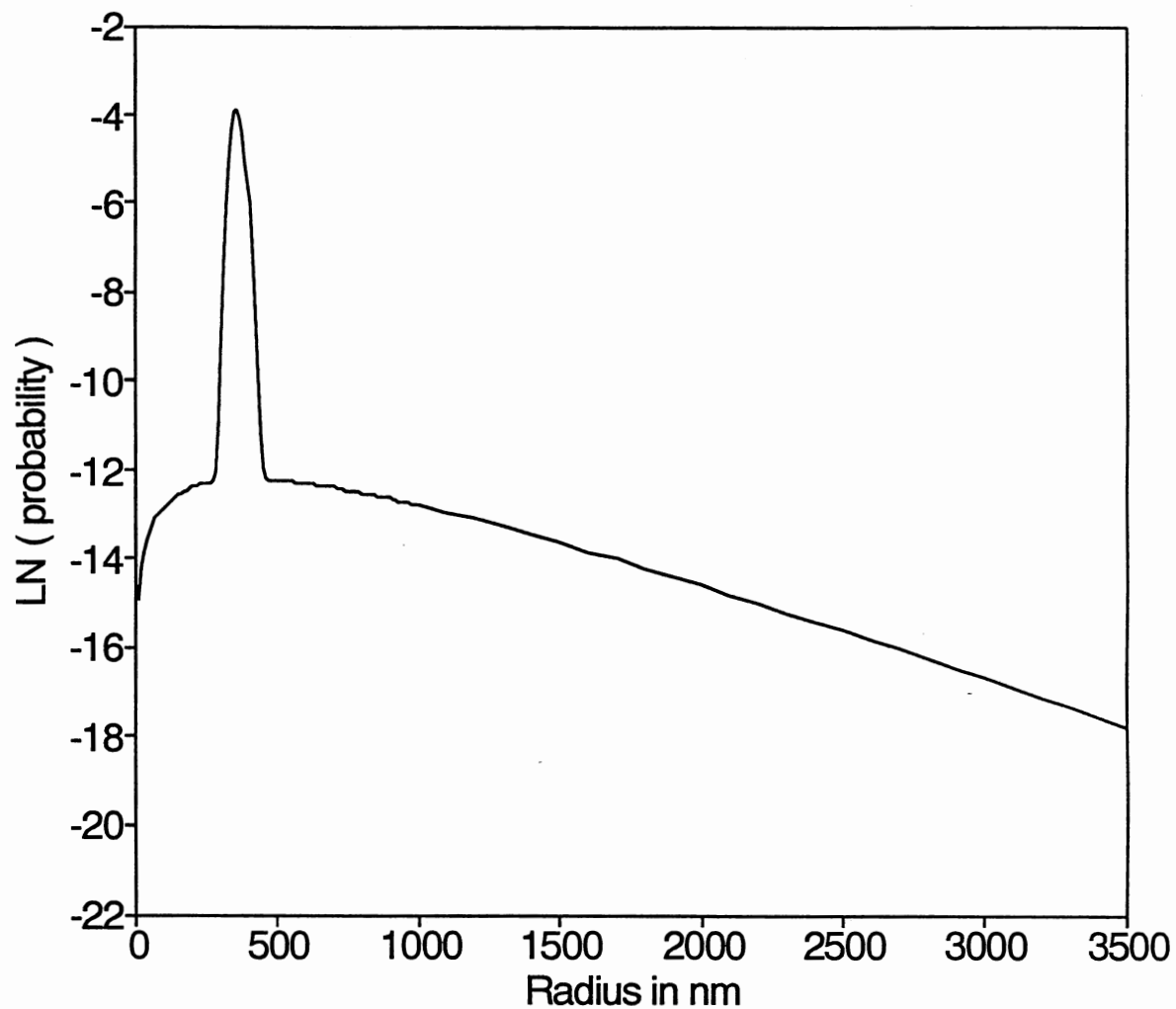
Figure 14. Particle Size Distribution of PMMA in Water. The plot shows the natural log of the normalized probability of finding a particle versus the radius of that particle in nm. The distribution is calculated using $R_1 = 360$ nm, $R_2 = 800$ nm, $\kappa = 200$, $Z_1 = 350$, and $Z_2 = 1$.

TPM-silica in Ethanol

The angular dependence of the scattered intensity and of the apparent size of the TPM-silica sample are displayed in Figures 15 and 16 respectively. The minimum in the form factor is the first one occuring when going from small to large scattering angles. The position of the minimum for the model form factor does not exactly coincide with the measured minimum. However the maximum of the apparent size in Figure 16 fits very well. Since the scattering intensity is very low at the form factor minimum, noise influences the correlation function more at these angles. This is obvious in Figure 17 where the signal to noise ratio is plotted as a function of $\sin(\theta/2)$. The signal to noise ratio looks very much like a mirror image of Figure 16: at the form factor minimum, the signal from the main particles decreases and allows more noise from the polydisperse bigger particles into the photomultiplier.

Polystyrene in Water: PST 500

This sample of polystyrene showed the familiar behavior for the form factor displayed in Figure 18. The apparent size on the other hand is not as sharply peaked as all previous samples: Figure 19 reveals that the radii obtained from dynamic light scattering are almost constant $(273 +/- 10$ nm) over the angular range examined. The minimum displayed is the first minimum of the sample. The form factor can be fit to several parameter combinations. Here again the dynamic scattering results of Figure 13 influenced the decision towards the chosen set. The fit with Equation 83 tries to suggest that the average radius of the particles is 280 nm, but the shape of the size distribution can be better described by 2 Schulz distributions; one corresponding to a polydispersity of $\sigma \approx 3$ % and the other one with $\sigma \approx 60$ % .

Figure 15. Form Factor of TPM-silica in Ethanol. The natural logarithm of the scattered intensity is plotted versus $\sin(\theta/2)$. The fit (solid line) is calculated using $\overline{R_1} = 250$ nm, $\overline{R_2} = 600$ nm, $\kappa = 200$, $Z_1 = 350$, and $Z_2 = 1$.
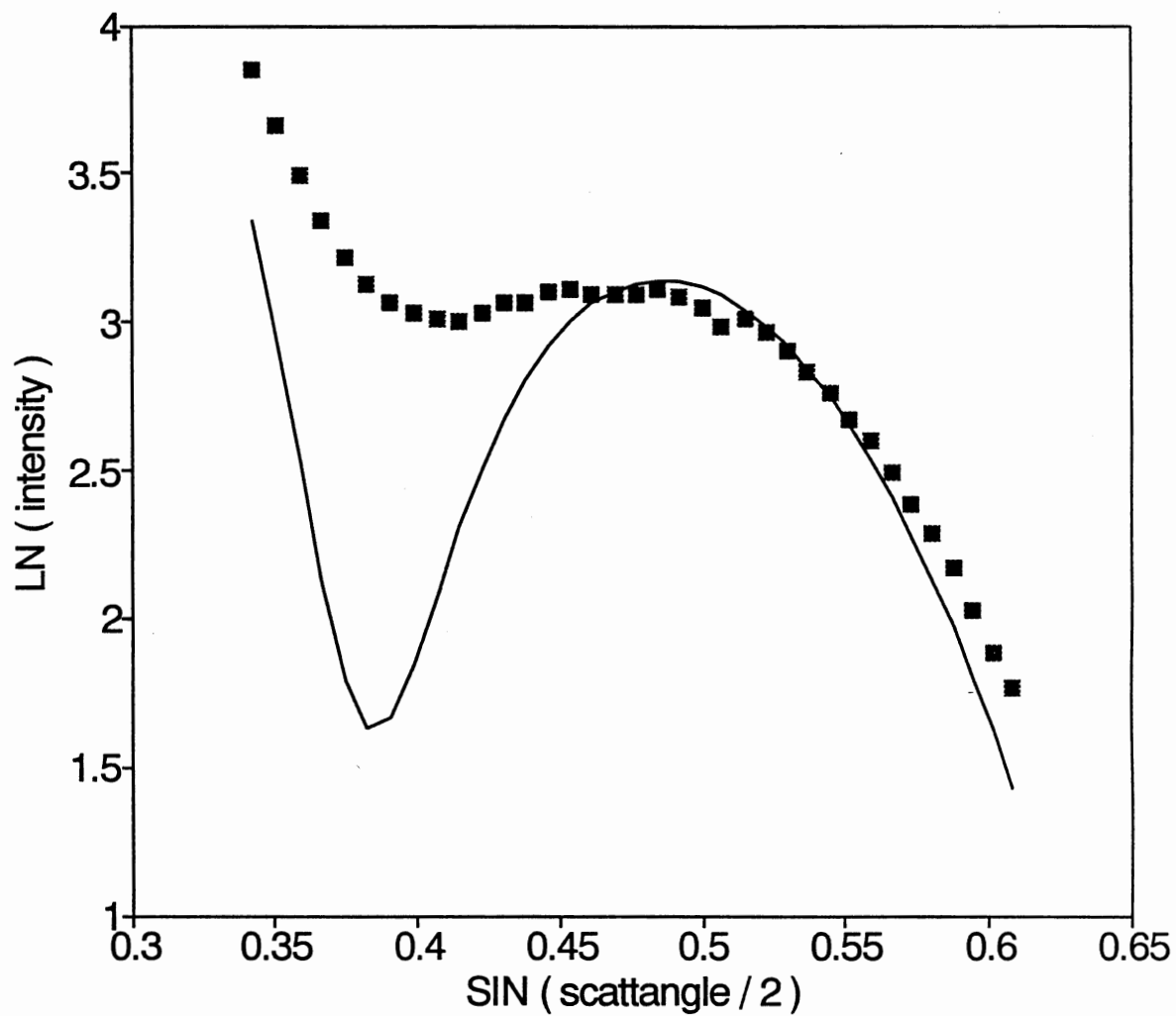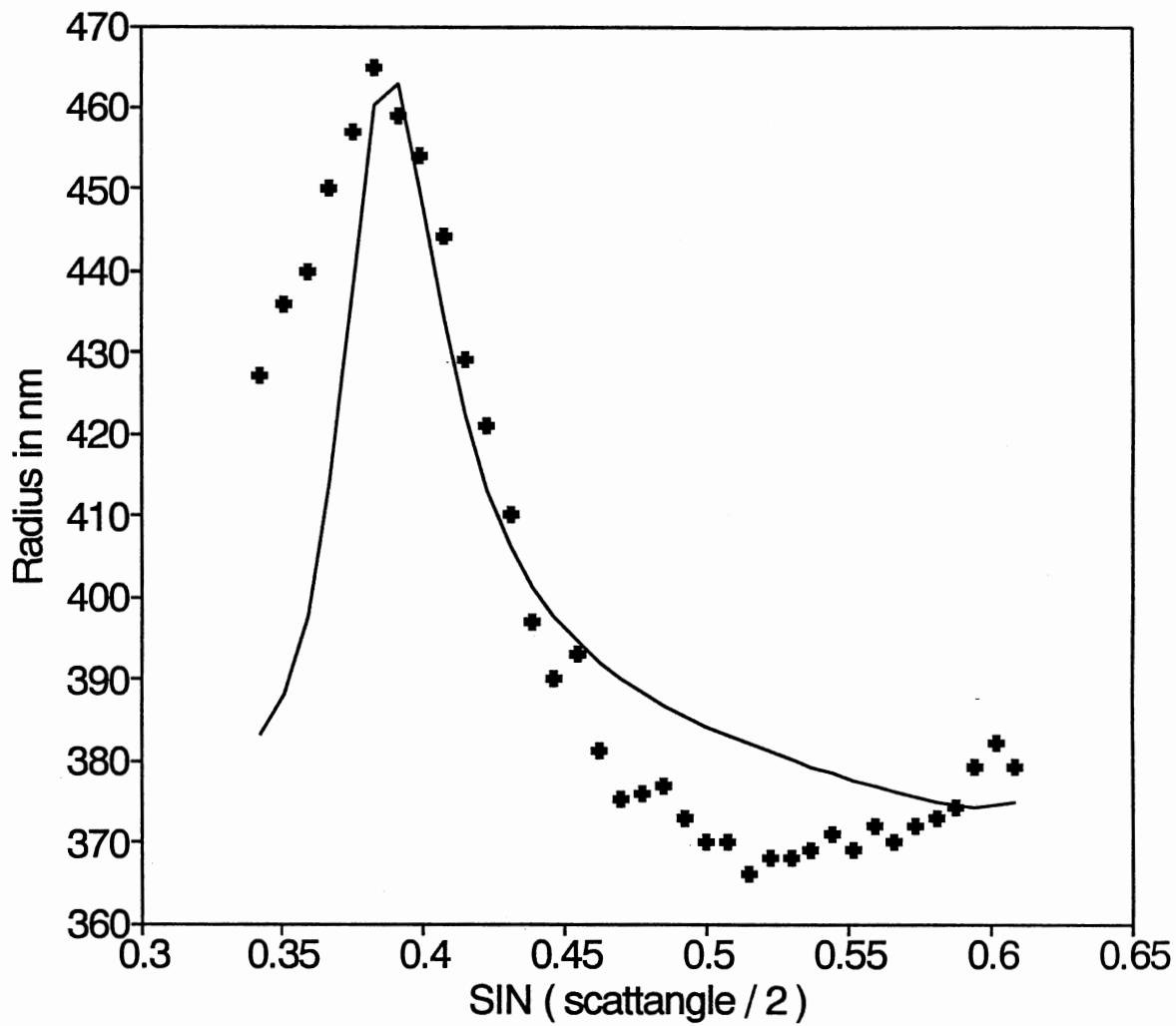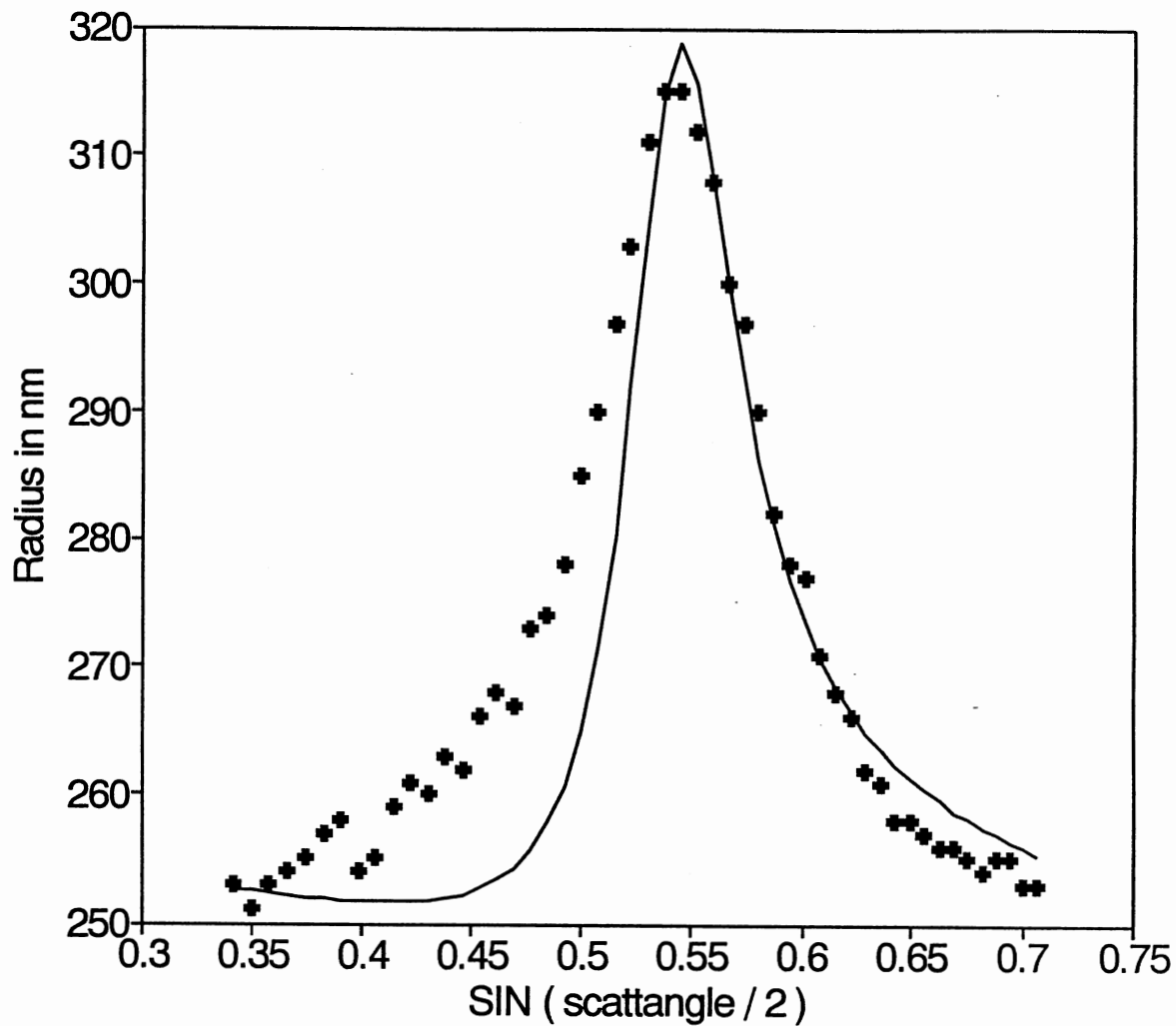
Figure 16. Dynamic Radius versus $\sin(\theta/2)$ of TPM-silica in Ethanol. The fit (solid line) is calculated using $\overline{R_1} = 250$ nm, $\overline{R_2} = 600$ nm, $\kappa = 200$, $Z_1 = 350$, and $Z_2 = 1$.

Figure 17. Signal to Noise Ratio of TPM-silica in Water. The intercepts of the measured intensity correlation functions are plotted versus $\sin(\theta/2)$.
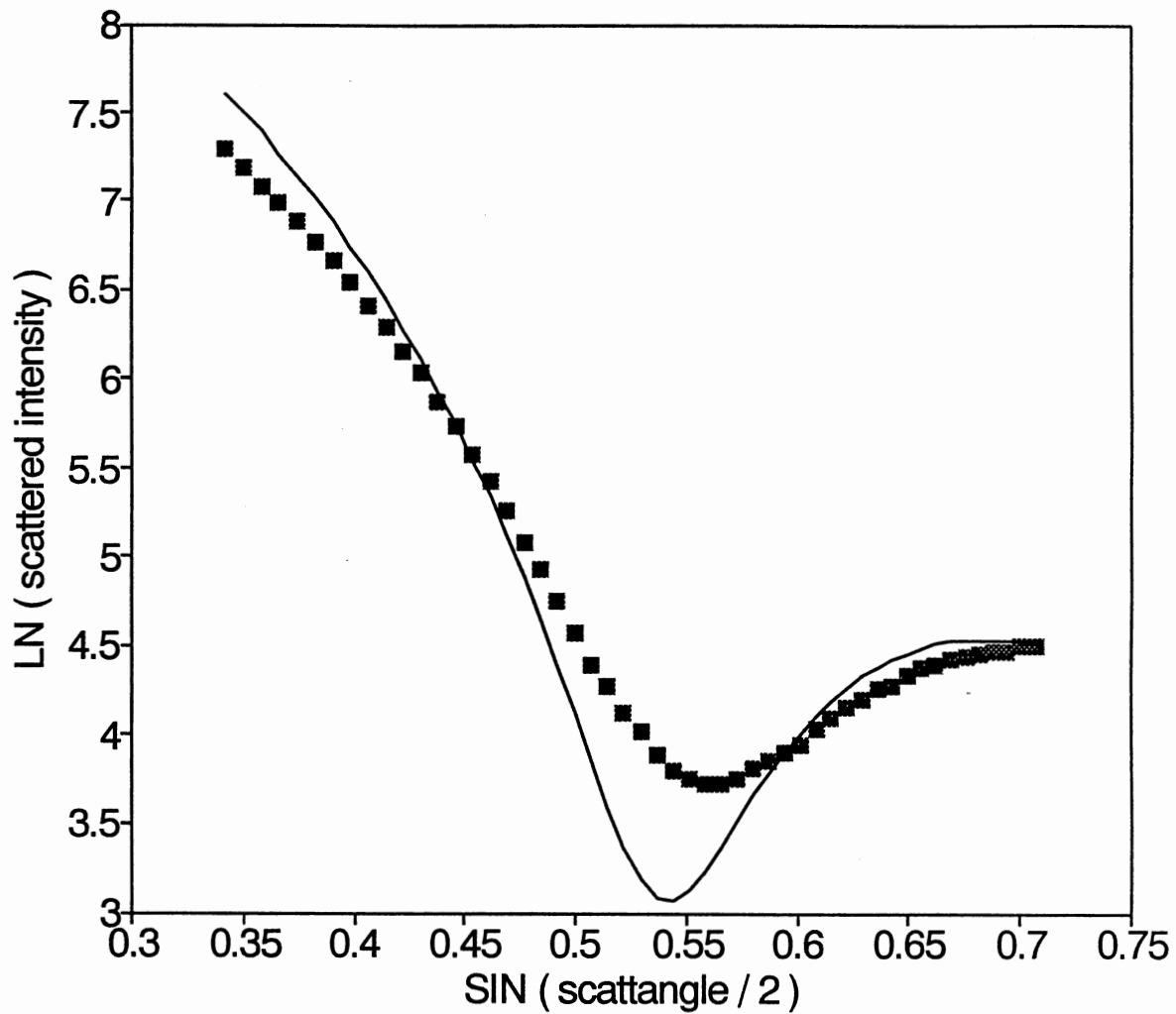
Figure 18. Form Factor of Polystyrene in Water: PST 500. The natural logarithm of the scattered intensity is plotted versus $\sin(\theta/2)$. The fit (solid line) is calculated using $\overline{R_1} = 280$ nm, $\overline{R_2} = 280$ nm, $\kappa = 50$, $Z_1 = 1000$, and $Z_2 = 2$.
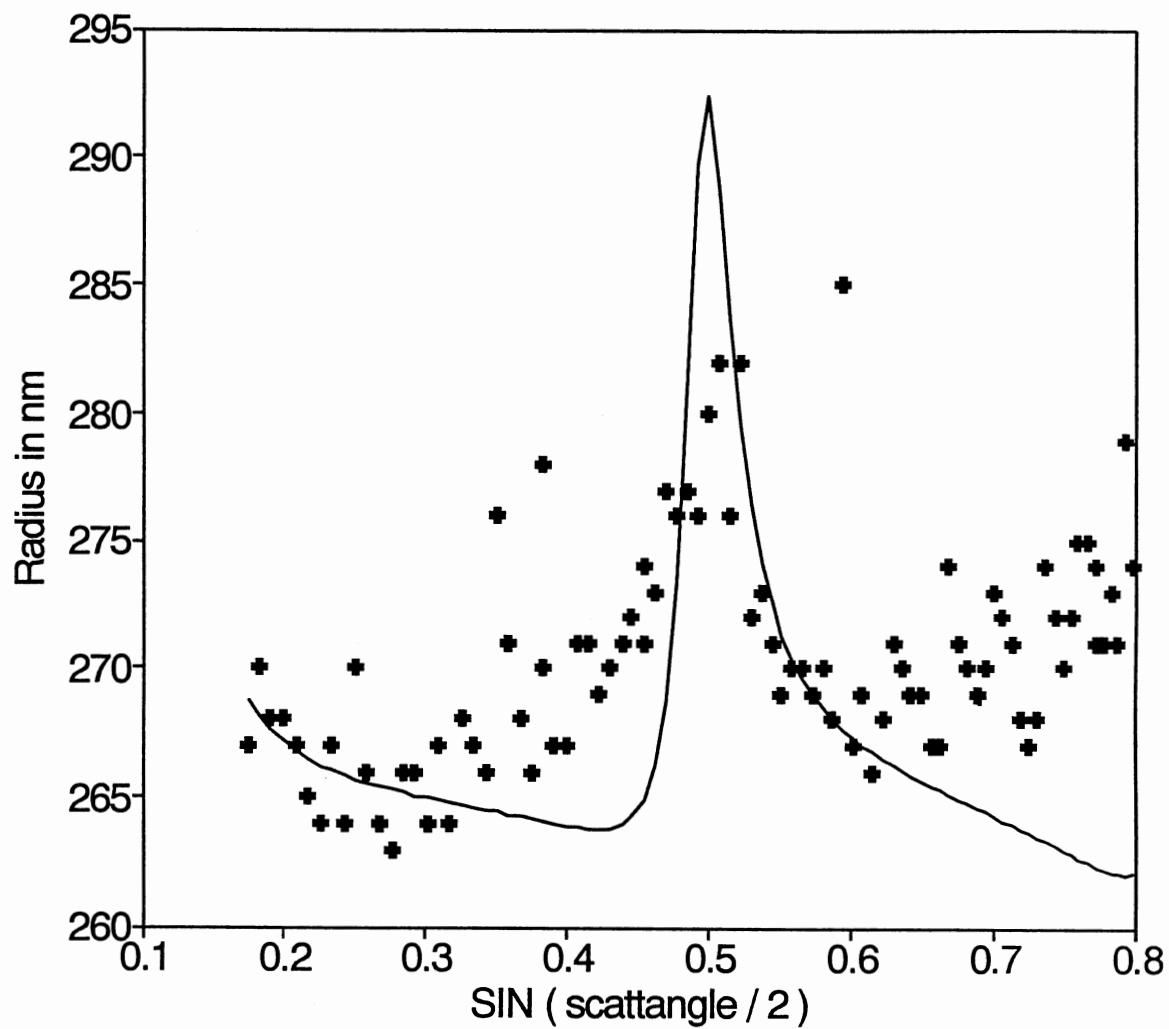
Figure 19. Dynamic Radius versus $\sin(\theta/2)$ of Polystyrene in Water: PST 500. The fit (solid line) is calculated using $\overline{R_1} = 280$ nm, $\overline{R_2} = 280$ nm, $\kappa = 50$, $Z_1 = 1000$, and $Z_2 = 2$.
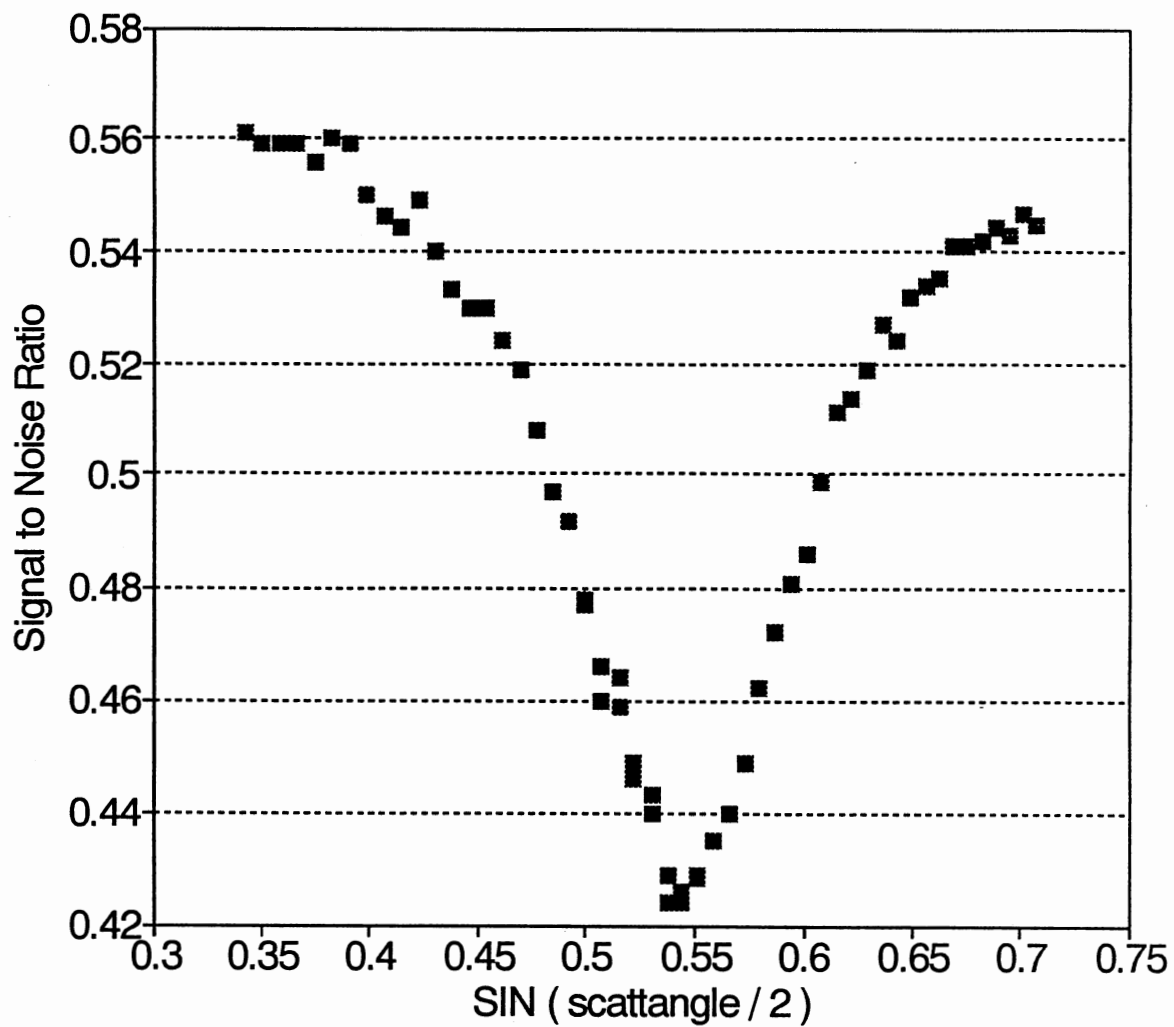
Polystyrene in Water: PST 600

The sample 'PST 600' seemed to be the one closest to a monodisperse suspension. The form factor (Figure 20) and the apparent size (Figure 21) could both be fit to a single Schulz distribution (Equation 34). The "quality" of the suspension displays itself in Figure 21: the radii obtained from dynamic light scattering lie within 2% of their mean value. The fit was calculated using $Z = 1000$ which corresponds to a polydispersity of $\sigma \approx 3\%$. Figure 21 shows why a single Schulz distribution does not explain the results of the other (PMMA, TPM-silica, and Polystyrene) samples: a single Schulz distribution *always* displays a jump from smaller than average to larger than average sizes in the apparent size. This can be explained intuitively: if the particles with the mean radius have their intensity minimum at an angle η, then particles with a radius slightly higher will have their minimum at an angle smaller than η. The opposite is true for those particles having a radius slightly smaller than the mean. Thus by measuring a correlation function at an angle $\eta - \delta$, where δ is a small positive angle, the scattering of the larger particles is suppressed, i.e. the obtained intensity averaged radius is *smaller* than the mean radius. The dynamic radius at an angle $\eta + \delta$ is *bigger* than the mean because of the similar argument for smaller particles.

Polystyrene in Water: PST 600/1000

The sample 'PST 600' was contaminated with 10% polystyrene spheres of radius $R \approx 500nm$. Since 'PST 600' had proven to be very monodisperse (see previous paragraph), an experiment involving a two-component suspension should show the expected behavior of the apparent size and the intensity. Figure 22 contains a plot of the form factor of the mixture of the two polystyrene samples. The double Schulz model fits both the static scattering and the dynamic scattering (Figure 23) fairly well. It is not clear why the apparent size at the first maximum fluctuates more than would be expected from the experiments with samples other than polystyrene. Philipse and Vrij [21] reported measurements of the diffusion constant versus scattering vector for a polystyrene mix. Their sample had mainly
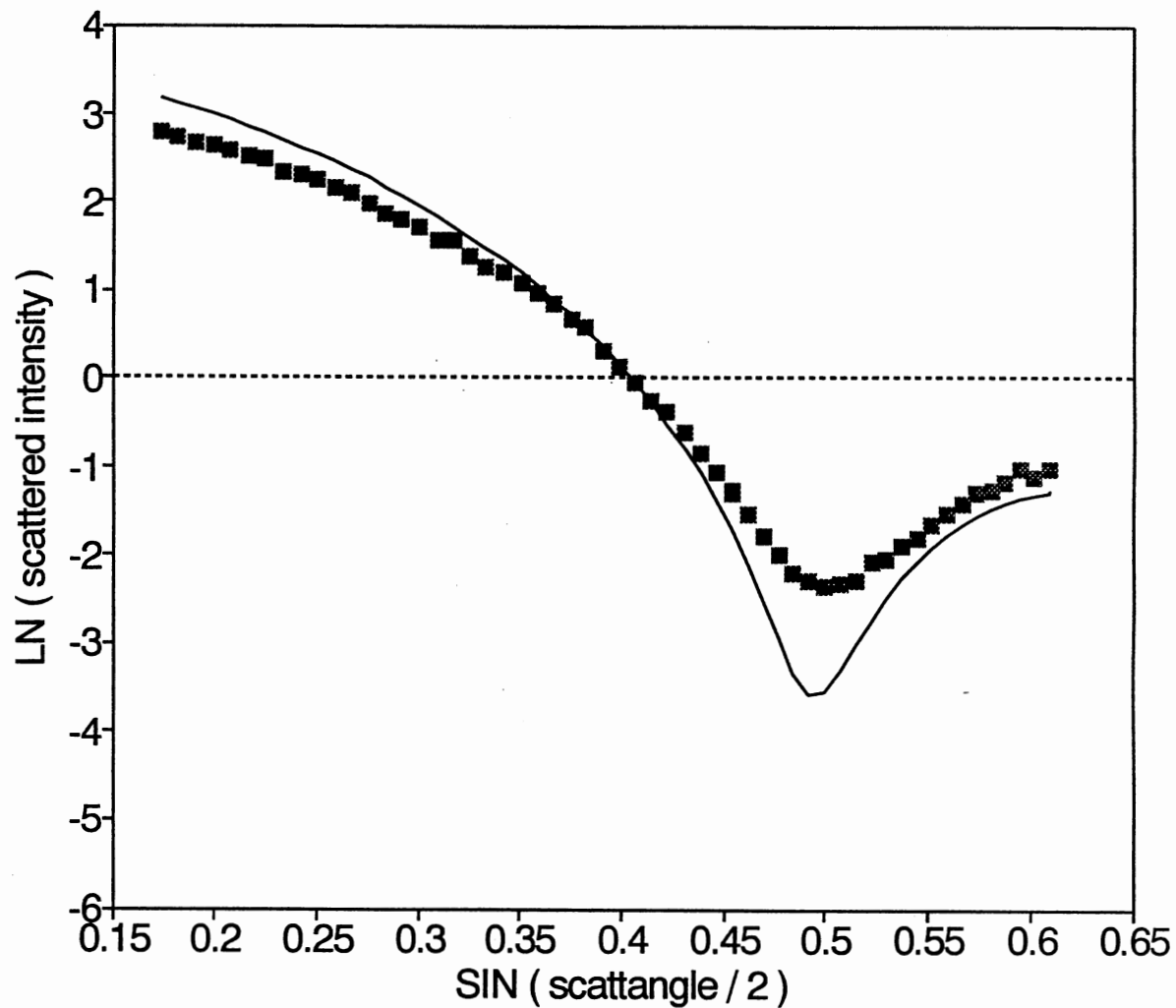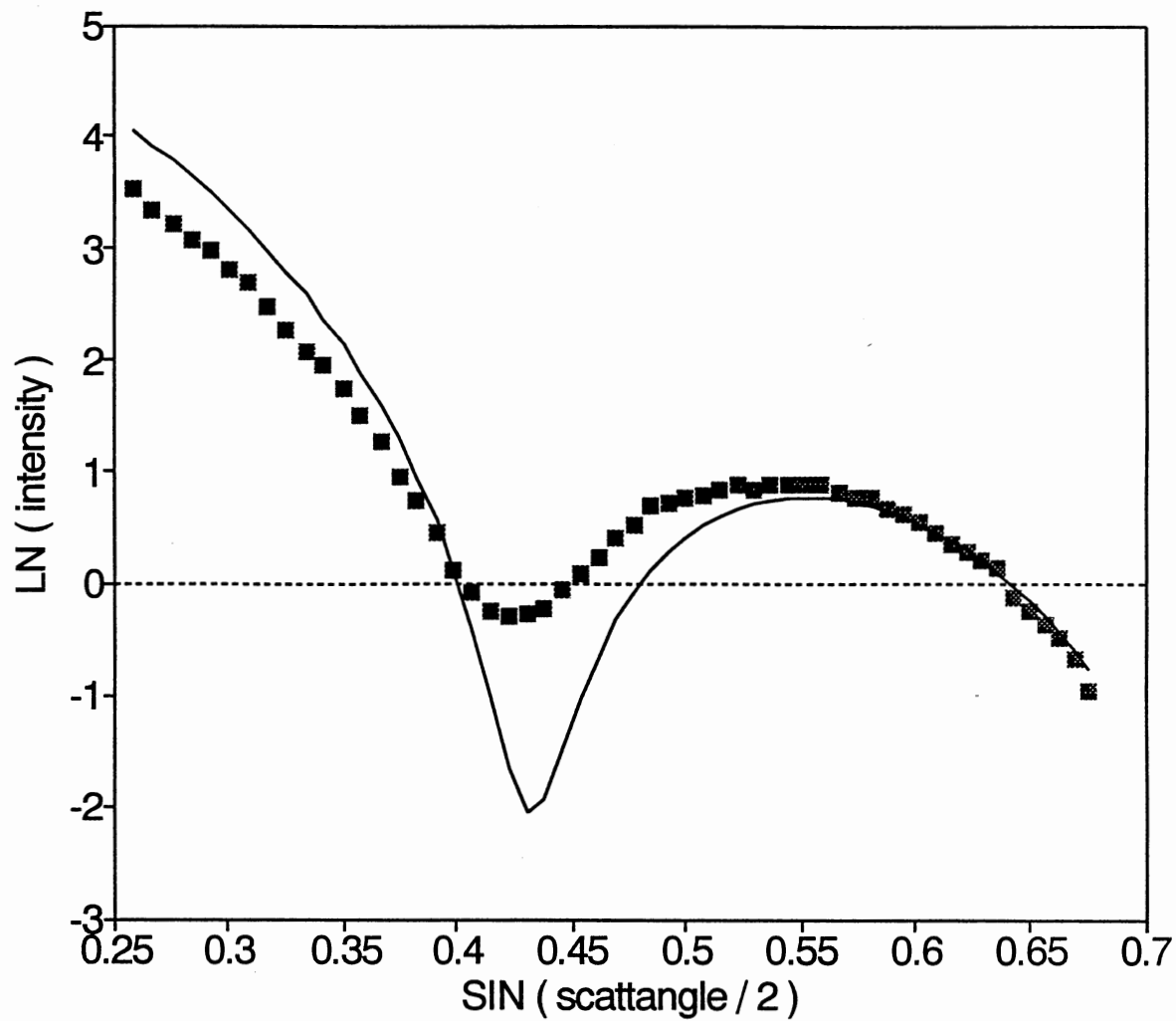
Figure 20. Form Factor of Polystyrene in Water: PST 600. The natural logarithm of the scattered intensity is plotted versus $\sin(\theta/2)$. The fit (solid line) is calculated using $\overline{R} = 320$ nm and $Z = 1000$.
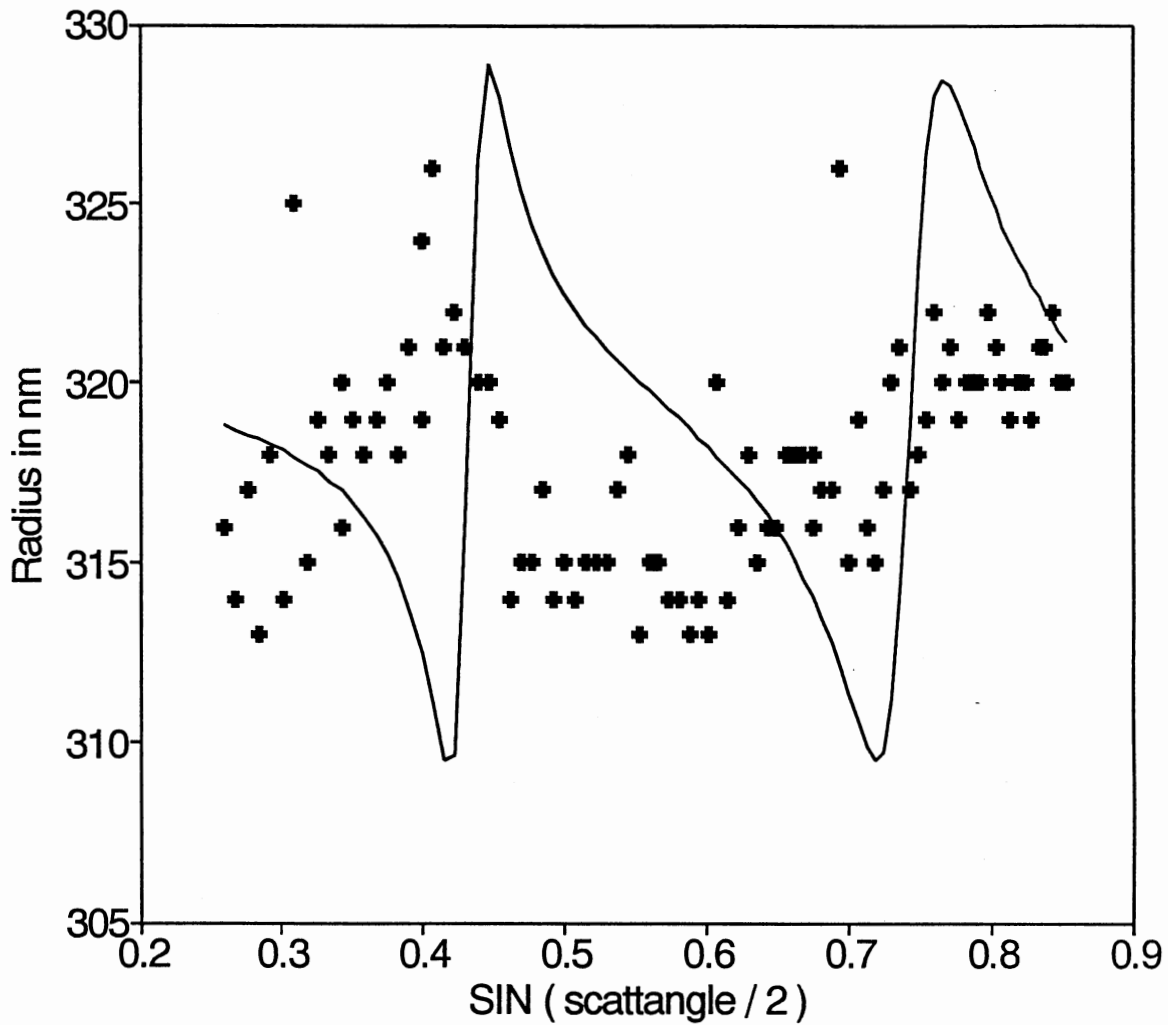
Figure 21. Dynamic Radius versus $\sin(\theta/2)$ of Polystyrene in Water: PST 600. The fit (solid line) is calculated using $\overline{R} = 320$ nm and $Z = 1000$.
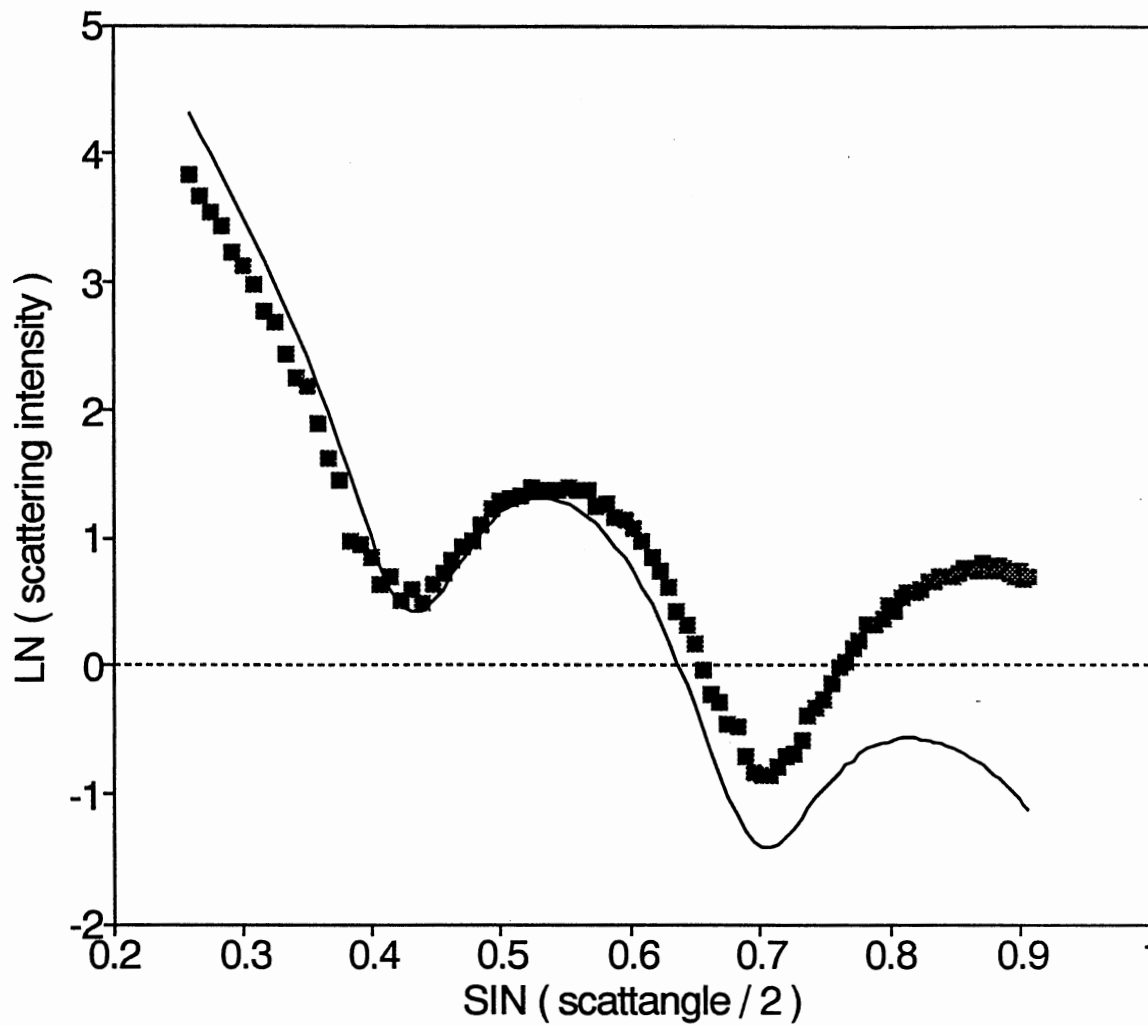
Figure 22. Form Factor of Polystyrene in Water: PST 600/1000. The natural logarithm of the scattered intensity is plotted versus $\sin(\theta/2)$. The fit (solid line) is calculated using $\overline{R_1} = 335$ nm, $\overline{R_2} = 500$ nm, $\kappa = 10$, $Z_1 = 450$, and $Z_2 = 350$.
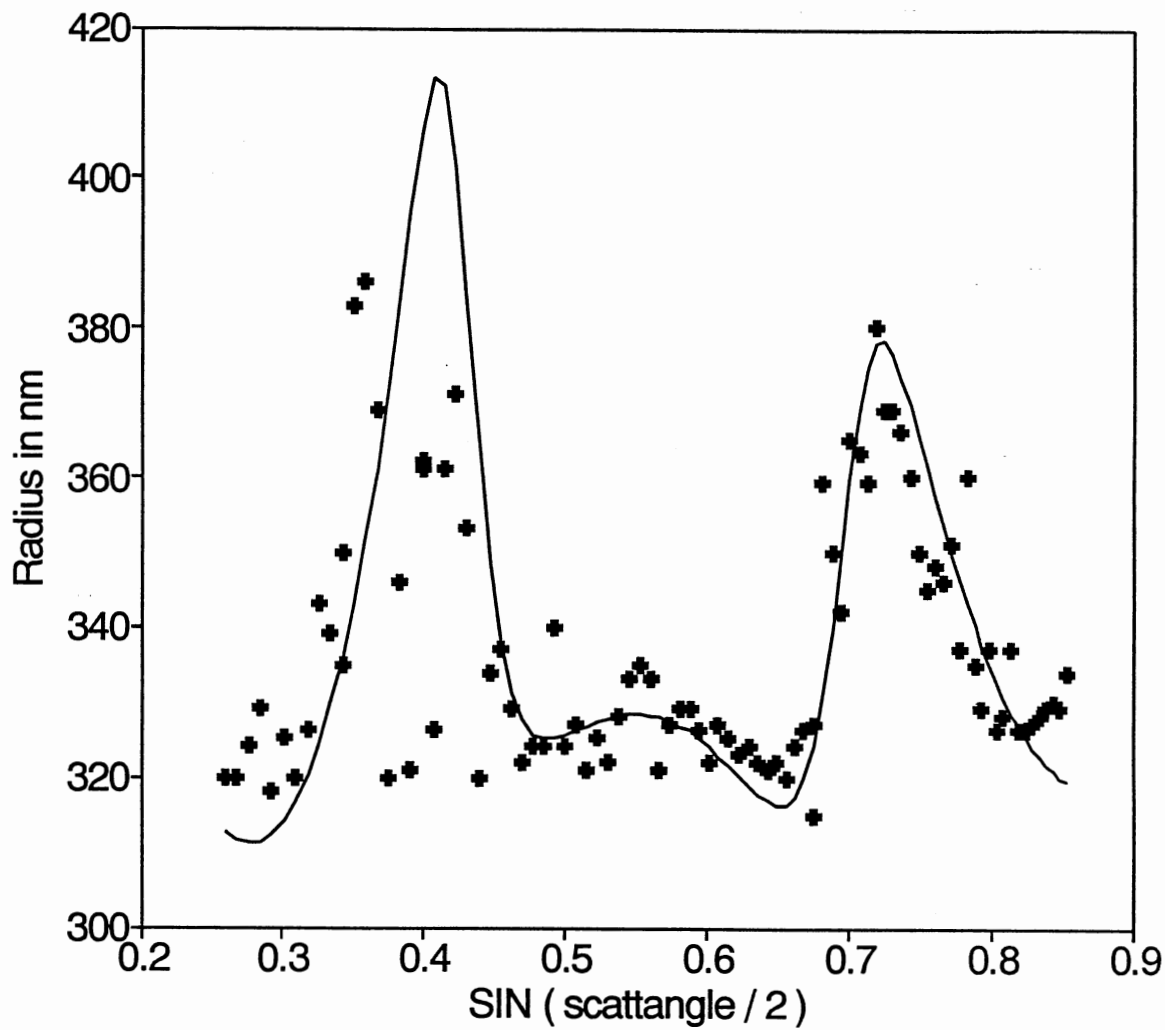
Figure 23. Dynamic Radius versus $\sin(\theta/2)$ of Polystyrene in Water: PST 600/1000. The fit (solid line) is calculated using $\overline{R_1} = 335$ nm, $\overline{R_2} = 500$ nm, $\kappa = 10$, $Z_1 = 450$, and $Z_2 = 350$.

big particles and a few small particles (controlled growth experiments). As a result they observe the opposite effect: at the minimum of the big particles the apparent size has a minimum as well. They however present no particle size distribution fit. A summary of the fitting constants used for the explanation of the dynamic radii of all samples is given in Table I.

TABLE I

FITTING CONSTANTS* FOR THE SAMPLES WITH
DOUBLE SCHULZ SIZE DISTRIBUTION

| Sample	Figure	κ	$\overline{R_1}$ in nm	Z_1	$\overline{R_2}$ in nm	Z_2
PMMA in Decalin	3	200	495	350	2000	5
PMMA in Tetralin	7	200	470	350	1700	10
PMMA in Dectet	3	200	480	350	1400	10
PMMA in CS$_2$	11	200	485	350	3000	5
PMMA in Water	13	200	360	350	800	1
TPM-silica in Ethanol	16	200	250	350	600	1
PST 500 in Water	19	50	280	1000	280	2
PST 600 in Water†	21	∞	320	1000		
PST 600/1000 in Water	23	10	335	450	500	350

* The constants are taken from Equation 83 .
† This sample was fit to a single Schulz distribution.

Discussion

The results shown in the previous section indicate that it is not possible to fit the scattering data of all PMMA and the TPM samples with Equations 48 and 56, which assume a single Schulz distribution of particle sizes in the samples. Pusey and van Megen presented that approach as a possible procedure for detecting small polydispersities [9]. They show apparent size data of PMMA spheres with a mean radius $\overline{R} \approx 590$ nm — particles very similar to the ones used in this study. However the data shown in reference [9] do not span such a wide range of $q \cdot R$ as presented here. Figure 24 contains the data already presented in Figure 3 but now with a fit calculated using the single Schulz distribution model (Equation 56) of Pusey and van Megen. This plot compares very well to the one presented in reference [9] if the data for $\sin(\theta/2) \lesssim 0.5$ are not taken into account, since Pusey and van Megen do not show data for the first and second minimum in the form factor for the 590 nm PMMA. They present static and dynamic results for another but smaller PMMA sample with $\overline{R} \approx 220$ nm. The apparent sizes from the correlation function measurements fit well to a single Schulz distribution near the first form factor 'minimum'. However the polydispersity of that sample was significantly higher ($\sigma \approx 11\%$) than the polydispersity of the samples of this report with $\sigma \approx 5\%$. The only other data set presented in reference [9] comes from a polystyrene sample with $\overline{R} \approx 179$ nm. The particles proved to be extremely monodisperse very much like the 'PST 600' sample investigated here.

From the comparison with reference [9], it seems that the single Schulz distribution does not always provide a good tool for determining small polydispersities. Especially for small polydispersities and big particles that show more than one minimum in the form factor, a double Schulz distribution allows a better fit to scattering data. The main fitting criterion is the apparent size from the cumulant fit to the intensity auto correlation function. At the minima of the form factor —when the scattered intensity of the main species of particles is very low —dynamic light scattering is very sensitive to contributions from other particle

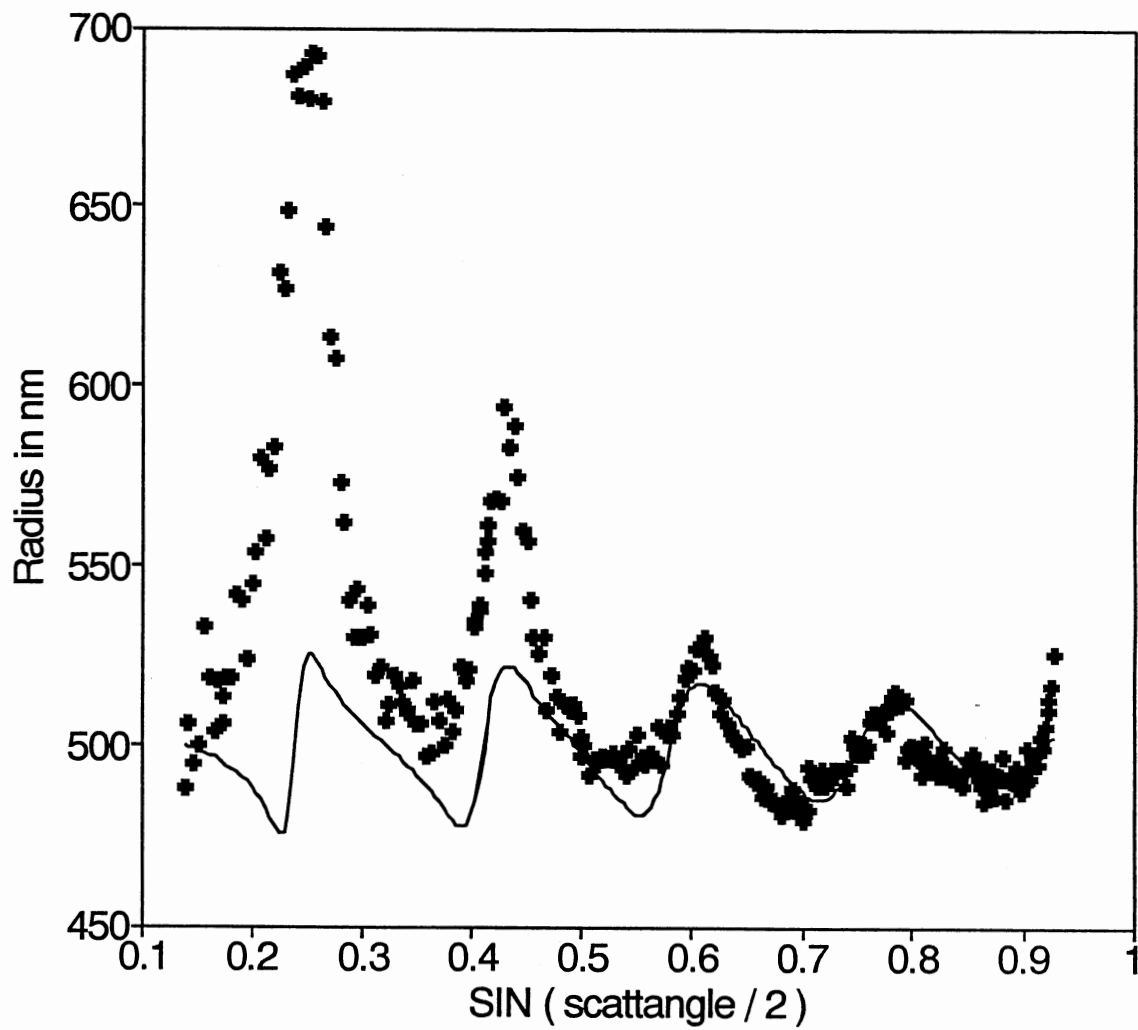Figure 24. Dynamic Radius versus $\sin(\theta/2)$ of PMMA in Decalin. The fit (solid line) is calculated using a single Schulz distribution with $\overline{R} = 520$ nm and $Z = 350$.

sizes in the scattering sample. Bigger particles seem to be favored at these angles due to the R^6-dependence of the scattered intensity (Equation 26). These larger particles might either be 'real' contributions from the particle size distribution or aggregates. An argument against the 'real' contributions is the fact that samples of the kind used in this study have not shown big particles under transmission electron microscopy. Aggregates on the other hand should show up as jumps in the count rates while measuring the correlation function. This was generally not the case, the count rate displayed only statistical fluctuations (due to Brownian motion of the particles into and out of the illuminated measuring volume in the sample).

The amplitudes of all intensity data in this study deviate more or less from the expected behavior, although the position of the form factor minima can be matched quite well. This deviation can only in part be explained with the additional solvent scattering, the background that was not substracted. Another contribution to the 'misfit' comes from the fact that for most particles of this study the Rayleigh-Gans-Debye criterion (Equation 22) does not hold: $\lambda \approx \overline{R} \Rightarrow 2ka(m-1) \approx 4\pi\triangle n \overset{?}{\ll} 1$. The difference of the index of refraction of the solvent and of the particle is denoted as $\triangle n$. For PMMA in decalin and in tetralin the refractive index difference is $\triangle n \approx 0.03$ which results in a value of 0.38 for the RGD parameter $2ka(m-1)$. It is interesting that the scattering can still be described well with the RGD form factors although 0.38 is barely smaller than 1. For polystyrene the RGD criterion is definitely not fullfilled: $2ka(m-1) \approx \pi \overset{!}{>} 1$. Nevertheless the positions of the form factor minima are where they should be according to RGD theory. A more rigorous treatment should use the form factors from the general Mie theory [47]. As Pusey and van Megen [9] point out, the use of Mie theory instead of RGD form factors will result in a determination of a smaller size than expected from RGD theory. (This is also reported by Philipse, Smits, and Vrij [22] and by Pelssers [48].) They also remark that Mie theory generated form factors show more shallow minima — as observed for many samples in this study.

A method of obtaining the shape of the size distribution functions from the scattered data directly, that is without fitting 'by eye', is presented in Appendix B. An integral relationship can be used to invert the scattering data. The drawback however is the numerical evaluation of integrals involving the raw data as the integrand. Very accurate data at many scattering angles should be necessary to produce a detailed outcome. This method also assumes that the form factor is exactly the RGD form factor and has to be modified to work with a Mie form factor.

CHAPTER VI

SUMMARY AND CONCLUSIONS

The sizing of particles with a radius on the order of the wavelength of light plays an important part in today's science and has many applications. This work presents how detailed information about an ensemble of those particles can be extracted from scattering data.

Suspensions of several particle species were investigated by light scattering. The data obtained from the angular dependence of the scattered intensity and its autocorrelation function were fit to a model assuming that not all particles have the same size. The model particle size distribution functions differ from those reported in similar studies, especially at small scattering angles. A combination of two Schulz size distributions is found to explain most scattering results well.

Future research could consist of relaxing the RGD approximation (by using Mie form factors) and including anisotropy, more general particle shapes and polarization into the theory and testing the predicted behavior with scattering measurements on suitable particles. A different route could lead to the investigation of particle size distributions in concentrated samples where structure factors and multiple scattering complicate the situation.

BIBLIOGRAPHY

1. Brown, R.; *Phil. Mag.* **4**, 161 (1828).

2. Brown, R.; *Ann. Phys.* **14**, 294 (1828).

3. Tyndall, J.; *Phil. Mag.* **37**, 384 (1869).

4. Tyndall, J.; *Phil. Mag.* **38**, 156 (1869).

5. "Dynamic Light Scattering — Applications of Photon Correlation Spectroscopy" ed. by Pecora, R.; Plenum Press, New York (1985).

6. Pusey, P. N.; in "Liquids, Freezing and the Glass Transition", Les Houches Session LI, 1989, ed. by Levesque, D., Hansen, J.-P., and Zinn-Justin, J.; Elsevier, Amsterdam (1990).

7. Kerker, M.; "The Scattering of Light and other Electromagnetic Radiation"; Academic Press, New York (1969).

8. Schulz, G. V.; *Z. Phys. Chem.*, **43**, 25 (1935).

9. Pusey, P. N. and van Megen, W.; *J. Chem. Phys.* **80**, 3513 (1984).

10. Aragón, S. R. and Pecora, R.; *J. Chem. Phys.* **64**, 2395 (1976).

11. Tagami, Y. and Pecora, R.; *J. Chem. Phys.* **51**, 3293 (1969).

12. Kotlarchyk, M., Stephens, R. B., and Huang, J. S.; *J. Phys. Chem.* **92**, 1533 (1988).

13. Mazer, A. M., Benedek, G. B., and Carey, M. C.; *J. Phys. Chem.* **80**, 1075 (1976).

14. Koppel, D. E.; *J. Chem. Phys.* **57**, 4814 (1972).

15. Van Megen, W., Ottewill, R. H., Owens, S. M., and Pusey, P. N.; *J. Chem. Phys.* **82**, 508 (1985).

16. Brown, J. C., Pusey, P. N., Goodwin, J. W., and Ottewill, R. H.; *J. Phys. A: Math. Gen.* **8**, 664 (1975).

17. Dalberg, P. S., Bøe, A., Strand, K. A., and Sikkeland, T.; *J. Chem. Phys.* **69**, 5473 (1978).

18. Brown, J. C., Pusey, P. N., and Dietz, R.; *J. Chem. Phys.* **62**, 1136 (1975).

19. Pusey, P. N. and van Megen, W.; *J. Physique* **44**, 285 (1983).

20. Kops-Werkhoven, M. M. and Fijnaut, H. M.; *J. Chem. Phys.* **74** 1618 (1981).

21. Phillipse, A. P. and Vrij, A.; *J. Chem. Phys.* **87**, 5634 (1987).

22. Philipse, A. P., Smits, C., and Vrij, A.; *J. Colloid Interface Sci.* **129**, 335 (1989).

23. Wills, P. R.; *J. Phys. A (GB)* **14**, 3093 (1981).

24. Fijnaut, H. M.; *J. Chem. Phys* **74**, 6857 (1981).

25. Brehm, G. A. and Bloomfield, V. A.; *Macromolecules* **8**, 663 (1975).

26. Schmidt, M., Burchard, W., and Ford, N. C.; *Macromolecules* **11**, 452 (1978).

27. Berne, B. J.and Pecora, B.;"Dynamic Light Scattering", Wiley, New York (1976).

28. Jackson, J. D.; "Classical Electrodynamics", Wiley, New York (1975).

29. Stratton, J. A.; "Electromagnetic Theory", McGraw-Hill, New York (1941).

30. Strutt, J. W. (Lord Rayleigh); *Phil. Mag.* **41**, 107, 274, 447 (1871).

31. Lord Rayleigh; *Phil. Mag.* **47**, 375 (1899).

32. Weiner, B. B.; in "Modern Methods of Particle Size Analysis", ed. by Barth, H. G., Wiley, New York (1984).

33. Chu, B.; "Laser Light Scattering", Academic Press, New York (1974).

34. Siegert, A. J. F.; MIT Rad. Lab. Report #465 (1943).

35. Ackerson, B. J. and Clark, N. A.; *J. Physique* **42**, 929 (1981).

36. Tanford, C.; "Physical Chemistry of Macromolecules", Wiley, New York (1961).

37. Guinier, A.; *Ann. Phys.* **12**, 161 (1939).

38. Zimm, B. H.; *J. Chem. Phys.* **16**,1099 (1948).

39. Einstein, A.; *Ann. d. Phys.* **17**, 549 (1905).

40. Bargeron, C. B.; *J. Chem. Phys.* **61**, 2134 (1974).

41. Bantle, S., Schmidt, M., and Burchard, W.; *Macromolecules* **15**, 1604 (1982).

42. Antl, L., Goodwin, J. W., Hill, R. D., Ottewill, R. H., Owens, S. M., and Papworth, S.; *Colloids and Surfaces* **17**, 67 (1986).

43. Paulin, S. E. and Ackerson, B. J.; *Phys. Rev. Lett.* **64**, 2663 (1990).

44. Marković, I. and Ottewill, R. H.; *Colloid & Polymer Sci.* **264**, 65 (1986).

45. Pusey, P. N. and van Megen, W.; *Nature(London)* **320**, 340 (1986) and *Phys. Rev. Lett.* **59**, 2083 (1987).

46. Ottewill, R. H. and Livsey, I.; *Polymer* **28**, 109 (1987) .

47. Mie, G.; *Ann. Phys.* **25**, 377 (1908).

48. Pelssers, E.; "Single Particle Optimal Sizing", Thesis, Agricultural University of Wageningen (1988).

49. Gradsteyn, I. S. and Ryzhik, I. M.; "Table of Integrals, Series, and Products", Academic Press, New York (1980).

APPENDICES

APPENDIX A

THE INTEGRALS I_n, C_n, AND S_n

The generalized exponential or Schulz particle size distribution is given by Equation 34:

$$G_Z(a) = \frac{a^Z}{Z!}(\frac{Z+1}{\bar{a}})^{Z+1} \exp\left(-\frac{a}{\bar{a}}(Z+1)\right) , \tag{A.1}$$

where Z is the parameter describing the polydispersity. This distribution inserted into Equations 39–41

$$I_n = \int_0^\infty G(a)(qa)^n \, da , \tag{A.2}$$

$$C_n = \int_0^\infty G(a)(qa)^n \cos{(2qa)} \, da , \tag{A.3}$$

and

$$S_n = \int_0^\infty G(a)(qa)^n \sin{(2qa)} \, da , \tag{A.4}$$

produces integrals that have to be evaluated when finding the scattered intensity and the diffusion constant from a sample containing particles with a Schulz size distribution. Equation A.3 can be combined with A.4 to a new integral:

$$\begin{align}
E_n &:= C_n + iS_n \tag{A.5} \\
&= \int_0^\infty G(a)(qa)^n \exp{(i2qa)} \, da , \tag{A.6}
\end{align}$$

where Euler's equation

$$e^{ix} = \cos x + i \sin x \tag{A.7}$$

was used. After inserting $G(a)$ from Equation A.1 into the integral E_n an integral of the form

$$\int_0^\infty x^m e^{-x(v-iw)} \, dx \tag{A.8}$$

has to be solved. This can be done by repeated integration by parts:

$$
\begin{aligned}
\int_0^\infty x^m e^{-x(v-iw)}\, dx &= \left[\frac{-x^m e^{-x(v-iw)}}{v-iw}\right]_{x=0}^{x=\infty} - \frac{-1}{v-iw}m \int_0^\infty x^{m-1}e^{-x(v-iw)}\, dx \\
&= \frac{m}{v-iw}\int_0^\infty x^{m-1}e^{-x(v-iw)}\, dx \\
&\;\;\vdots \\
&= \frac{m!}{(v-iw)^m}\int_0^\infty e^{-x(v-iw)}\, dx \\
&= \frac{m!}{(v-iw)^m}\left[\frac{-1}{v-iw}e^{-x(v-iw)}\right]_{x=0}^{x=\infty} \\
&= \frac{m!}{(v-iw)^{m+1}}\; .
\end{aligned}
$$

(A.9)

Every complex number $v+iw$ can be written in terms of its distance from the origin ($\sqrt{v^2+w^2}$) and the angle between the real axis and the line connecting the origin with the point corresponding to the number in the complex plane ($\tan\phi = w/v$):

$$
v + iw = \sqrt{v^2+w^2}\, e^{i\arctan(\frac{w}{v})}\; .
$$

(A.10)

Taking the inverse of the complex conjugate of this expression gives :

$$
\frac{1}{v-iw} = \frac{1}{\sqrt{v^2+w^2}}e^{i\arctan(\frac{w}{v})}\; .
$$

(A.11)

Now Equation A.9 can be rewritten into

$$
\begin{aligned}
\int_0^\infty x^m e^{-x(v-iw)}\, dx &= m!\left(\frac{1}{v-iw}\right)^{m+1} \\
&= m!\left(\frac{1}{\sqrt{v^2+w^2}}e^{i\arctan(\frac{w}{v})}\right)^{m+1} \\
&= \frac{m!}{v^{m+1}\left(1+\frac{w^2}{v^2}\right)^{\frac{m+1}{2}}}e^{i(m+1)\arctan(\frac{w}{v})}\; .
\end{aligned}
$$

(A.12)

This is very useful in evaluating the integrals of Equations A.2–A.4.

For the integral I_n Equation A.12 can be applied with $w = 0$ and $v = (Z+1)/\bar{a}$:

$$
\begin{aligned}
I_n &= \left(\frac{Z+1}{\bar{a}}\right)^{Z+1}\frac{1}{Z!}\int_0^\infty (qa)^n \exp\left(-a\frac{(Z+1)}{\bar{a}}\right)a^Z\, da \\
&= \frac{q^n}{Z!}\left(\frac{Z+1}{\bar{a}}\right)^{Z+1}\frac{(Z+n)!}{\left(\frac{Z+1}{\bar{a}}\right)^{Z+n+1}} \\
&= \frac{(q\bar{a})^n}{(Z+1)^n}\frac{(Z+n)!}{Z!}
\end{aligned}
$$

(A.13)

and yields Equation 42.

The integral E_n (Equation A.6) can be solved similarly, only now with the substitution $w = 2q$ in Equation A.12:

$$
\begin{aligned}
E_n &= (\frac{Z+1}{a})^{Z+1}\frac{1}{Z!}\int_0^\infty (qa)^n \exp\left(-a(\frac{(Z+1)}{a} - i2q)\right)a^Z\, da \\
&= \frac{q^n}{Z!}(\frac{Z+1}{a})^{Z+1}\frac{(Z+n)!}{(\frac{Z+1}{a})^{Z+n+1}}(1 + (\frac{2q\bar{a}}{Z+1})^2)^{-\frac{Z+n+1}{2}} \\
&\qquad\qquad \times \exp\left\{i(Z+n+1)\arctan\left(\frac{2q\bar{a}}{Z+1}\right)\right\} \\
&= \frac{(q\bar{a})^n}{(Z+1)^n}\frac{(Z+n)!}{Z!}(1 + (\frac{2q\bar{a}}{Z+1})^2)^{-\frac{Z+n+1}{2}} \\
&\qquad\qquad \times \exp\left\{i(Z+n+1)\arctan\left(\frac{2q\bar{a}}{Z+1}\right)\right\} \\
&= I_n(1 + (\frac{2q\bar{a}}{Z+1})^2)^{-\frac{Z+n+1}{2}}\exp\left\{i(Z+n+1)\arctan\left(\frac{2q\bar{a}}{Z+1}\right)\right\}. \quad\text{(A.14)}
\end{aligned}
$$

But this result contains C_n and S_n because they are the real and imaginary parts of E_n:

$$
C_n = \Re(E_n) = I_n(1 + (\frac{2q\bar{a}}{Z+1})^2)^{-\frac{Z+n+1}{2}}\cos\left\{(Z+n+1)\arctan\left(\frac{2q\bar{a}}{Z+1}\right)\right\} \quad\text{(A.15)}
$$

$$
S_n = \Im(E_n) = I_n(1 + (\frac{2q\bar{a}}{Z+1})^2)^{-\frac{Z+n+1}{2}}\sin\left\{(Z+n+1)\arctan\left(\frac{2q\bar{a}}{Z+1}\right)\right\}. \quad\text{(A.16)}
$$

These are Equations 43 and 44.

APPENDIX B

INVERSE TRANSFORM FOR PARTICLE SIZE ANALYSIS

The form factor for a sphere in the RGD approximation is according to Equations 26 and 27

$$\frac{I(q)}{I_0} = a^6 P(qa) \ , \tag{B.1}$$

where

$$P(qa) = (\frac{3}{(qa)^3}(\sin{(qa)} - qa\cos{(qa)}))^2 \ .$$

Equation B.1 can be rewritten in terms of a spherical harmonic of order one. Since

$$j_1(qa) = \frac{\sin{(qa)}}{(qa)^2} - \frac{\cos{(qa)}}{qa} \tag{B.2}$$

the form factor can be expressed as :

$$\frac{I(q)}{I_0} = a^6(\frac{3j_1(qa)}{qa})^2 \ . \tag{B.3}$$

The first cumulant is defined as the negative slope of the field correlation function (see Equation 20):

$$\begin{aligned} \kappa_1 \ &:= \ -\lim_{\tau \to 0}\frac{\partial g^1(\tau)}{\partial \tau} = Dq^2 \\ &= \ \frac{k_B T}{6\pi\eta a}q^2 \ . \end{aligned} \tag{B.4}$$

Equation 28 was used to substitute the diffusion coefficient. If the correlation function contains contributions from particles with different sizes the measured value for κ_1 will be the intensity weighed average of all contributing cumulants:

$$\begin{aligned} \langle \kappa_1 \rangle \ &:= \ \int_0^\infty \kappa_1(qa)a^6 P(qa)N(a) \, da \\ &= \ \frac{3k_B T}{2\pi\eta} \int_0^\infty a^3 j_1^2(a)N(a) \, da \ , \end{aligned} \tag{B.5}$$

where $N(a)$ denotes the unknown size distribution. The average cumulant $\langle \kappa_1 \rangle$ can be measured with dynamic light scattering. An inverse transform is needed to determine the unknown function $N(a)$ from the cumulant data. An integral relation involving the Bessel/Neumann functions J_ν / N_ν can help solving this problem (formula 6.524.1 of reference [49]):

$$\int_0^\infty x J_\nu^2(ax) J_\nu(bx) N_\nu(bx)\, dx = \begin{cases} 0 & \text{if } 0 < a < b, \Re(\nu) > -\frac{1}{2} \\ -(2\pi ab)^{-1} & \text{if } 0 < b < a, \Re(\nu) > -\frac{1}{2} \end{cases}, \tag{B.6}$$

where $\Re(\nu)$ is the real part of ν. The Bessel/Neumann functions are related to the spherical harmonics via the following equations [7]:

$$J_{\nu+1/2}(ax) = \sqrt{\frac{2ax}{\pi}} j_\nu(ax) \quad \text{and} \quad N_{\nu+1/2}(ax) = \sqrt{\frac{2ax}{\pi}} n_\nu(ax) \ . \tag{B.7}$$

Thus for the special case of spherical harmonics of order 1 the integral in Equation B.6 becomes:

$$\int_0^\infty \frac{4ab}{\pi^2} x^3 j_1^2(ax) j_1(bx) n_1(bx)\, dx = \begin{cases} 0 & \text{if } 0 < a < b \\ -(2\pi ab)^{-1} & \text{if } 0 < b < a \end{cases}$$

$$\Rightarrow \quad \int_0^\infty x^3 j_1^2(ax) j_1(bx) n_1(bx)\, dx = \begin{cases} 0 & \text{if } 0 < a < b \\ -\frac{\pi}{8a^2 b^2} & \text{if } 0 < b < a \end{cases}. \tag{B.8}$$

The function n_1 is given by

$$n_1(qa) = -\frac{\cos(qa)}{(qa)^2} - \frac{\sin(qa)}{qa} \tag{B.9}$$

and is orthogonal to j_1. The explicit result of Equation B.8 will be used to evaluate the integral W defined by:

$$W(b) := \int_0^\infty q^3 j_1(qb) n_1(qb) \langle \kappa_1(qa) \rangle\, dq \ . \tag{B.10}$$

With this definition $W(b)$ becomes:

$$\begin{aligned} W(b) &= \frac{3kT}{2\pi\eta} \int_0^\infty \int_0^\infty a^3 j_1^2(qa) N(a) q^3 j_1(qb) n_1(qb)\, dk\, da \\ &= \frac{3kT}{2\pi\eta} \int_b^\infty a^3 N(a) \{ -\frac{\pi}{8a^2 b^2} \}\, da \\ &= -\frac{3kT}{16\eta b^2} \int_b^\infty a N(a)\, da \ , \end{aligned} \tag{B.11}$$

or after bringing the factors to the left side:

$$\frac{16\eta b^2}{3kT}W(b) = -\int_b^\infty aN(a)\,da \ . \tag{B.12}$$

This equation can be differentiated with respect to b on both sides:

$$\frac{d}{db}\left\{\frac{16\eta b^2}{3kT}W(b)\right\} = -\frac{d}{db}\left\{\int_b^\infty aN(a)\,da\right\} = bN(b) \ . \tag{B.13}$$

With this procedure an expression for $N(b)$ — the particle size distribution — is obtained.

$$N(b) = \frac{1}{b}\frac{d}{db}\left\{\frac{16\eta b^2}{3kT}W(b)\right\} \ , \tag{B.14}$$

where the function $W(b)$ is given in Equation B.10 .

In operator notation Equation B.14 can be rewritten as:

$$\begin{aligned}
N(b) &= \frac{16\eta}{3kT}\left[\frac{1}{b}\frac{d}{db}\left\{b^2\int_0^\infty q^3 j_1(qb)n_1(qb)\langle\kappa_1(q)\rangle\,dq\right\}\right]\\
&= \frac{16\eta}{3kT}\left[\int_0^\infty q^3\mathcal{O}^-\langle\kappa_1(q)\rangle\,dq\right] \ ,
\end{aligned} \tag{B.15}$$

where the operator $\mathcal{O}^-$ is defined by

$$\mathcal{O}^- := \frac{1}{b}\frac{d}{db}\{b^2 j_1(qb)n_1(qb)\} \ . \tag{B.16}$$

This operator is an inverse operator that works on the raw scattering data $\langle\kappa_1(q)\rangle$ such that the size distribution is produced after an integration over all q, the scattering vectors.

Limiting Case for $q \to \infty$

    The convergence properties of the integral describing $N(b)$ in Equation B.15 are of interest. To investigate the behavior at large scattering vectors the $(q \to \infty)$-limits of the spherical harmonics (Equations B.2 and B.9)

$$j_1(qa) = \frac{\sin(qa)}{(qa)^2} - \frac{\cos(qa)}{qa} \qquad n_1(qa) = -\frac{\cos(qa)}{(qa)^2} - \frac{\sin(qa)}{qa}$$

can be used:

$$j_1(qa) \xrightarrow{q\to\infty} -\frac{\cos(qa)}{qa} \qquad n_1(qa) \xrightarrow{q\to\infty} -\frac{\sin(qa)}{qa} \ . \tag{B.17}$$

Since there are no b-dependent functions behind the operator $\mathcal{O}^-$ in Equation B.15 the operator becomes

$$\mathcal{O}^- \overset{q\to\infty}{\longrightarrow} \frac{1}{b}\frac{d}{db}b^2\frac{\cos(qb)\sin(qb)}{(qb)^2} = \frac{1}{b}\frac{d}{db}\frac{\sin(2qb)}{2q^2} = \frac{\cos(2qb)}{qb}\; , \tag{B.18}$$

where the definition of $\mathcal{O}^-$ in Equation B.16 was used. The first cumulant

$$\langle\kappa_1(q)\rangle = \int_0^\infty \frac{k_B T}{6\pi\eta a}q^2 a^6 P(qa)N(a)\,da$$

approaches the limit

$$\langle\kappa_1(q)\rangle \overset{q\to\infty}{\longrightarrow} \int_0^\infty \frac{3k_B T}{2\pi\eta a}a^2\frac{\cos^2(qa)}{q^2}N(a)\,da\; , \tag{B.19}$$

where the limit

$$P(qa) = \frac{9j_1(qa)}{(qa)^2} \overset{q\to\infty}{\longrightarrow} \frac{9\cos^2(qa)}{(qa)^4}$$

was used in the calculation. Now the particle size distribution can be expressed by:

$$N(b) = \int_0^\infty \cos(2qb)\cos^2(qa)\frac{a}{b}\,dq\; , \tag{B.20}$$

where Equations B.15 , B.18 and B.19 have been applied. This result is "something like a Delta-function". Only for $a = b$ will this integral have a value, for all other $a \neq b$ the integral in Equation B.20 will be zero. Unfortunately Equation B.20 points out one disadvantage: the integrand is *not* converging and thus even large q-values contribute to the integral. This means that the integral cannot be cut off at some q without losing considerable parts of the integral. Any experiment however has one maximum q determined by the maximum scattering angle (that can not be larger than 180 degrees).

The Case of Polydisperse Samples

For a polydisperse sample, the total form factor is a sum of the individual form factors corresponding to the different sizes. Since those form factors are only sin - and cos -functions, the summation of these oscillating parts will average out to zero. This argumentation leads to the limit

$$\left(\frac{\sin x}{x^3} - \frac{\cos x}{x^2}\right)^2 \overset{x\to\infty}{\longrightarrow} \frac{1}{x^4} \qquad \text{or:} \qquad a^6 P(qa) \overset{q\to\infty}{\longrightarrow} a^6\frac{9}{(qa)^4} = \frac{9a^2}{q^4} \tag{B.21}$$

for the intensity weighted form factor. With this expression and the limit of the inverse operator $\mathcal{O}^-$ (Equation B.18) the size distribution of Equation B.15 is:

$$
\begin{aligned}
N(b) \quad &= \quad \frac{16\eta}{3kT} \int_0^\infty q^3 \mathcal{O}^- \langle \kappa_1(q) \rangle \, dq \\
&\cong \quad \frac{16\eta}{3kT} \int_0^\infty q^3 \frac{\cos(2qb)}{qb} \frac{9a^2}{q^4} \frac{k_B T}{6\pi\eta a} q^2 \, dq \\
&\cong \quad \frac{8a}{\pi b} \int_0^\infty \cos(2qb) \, dq \\
&\overset{\text{``}}{\cong} \quad \frac{4a}{\pi b^2} [\sin(2qb)]_{(0)}^{(\infty)} \text{''} \quad ,
\end{aligned}
\tag{B.22}
$$

which is not as badly defined as the single sphere case. It should be possible to combine two techniques:

First fit the experimental results to a known size distribution that matches the data well at the largest scattering angles down to an angle corresponding to the wave vector q_{max}.

Then apply the inverse operator technique to the nonmatching difference caused by additional particle sizes in the sample.

If the experimental cumulant data, the calculated cumulants and the difference between the two are denoted by $\langle \kappa_1 \rangle_{exp}$, $\langle \kappa_1 \rangle_{fit}$, and $\langle \kappa_1 \rangle_\delta$ respectively, then the equation

$$
\langle \kappa_1 \rangle_\delta = \langle \kappa_1 \rangle_{exp} - \langle \kappa_1 \rangle_{fit}
\tag{B.23}
$$

should hold by definition of the quantities involved. The size distribution

$$
N_{exp}(b) = \frac{16\eta}{3kT} \int_0^\infty q^3 \mathcal{O}^- \langle \kappa_1 \rangle_{exp} \, dq
\tag{B.24}
$$

is easily seen to be composed of two parts:

$$
N_{exp}(b) = N_{fit}(b) + N_\delta(b) \ .
\tag{B.25}
$$

The function $N_{fit}(b)$ was chosen to produce a good fit to the cumulant data for scattering angles larger than a maximum angle corresponding to a wave vector

q_{max}. Thus $N_{fit}(b)$ is *known*. $N_\delta(b)$ on the other hand can be calculated without any convergence trouble:

$$N_\delta(b) = \frac{16\eta}{3kT} \int_0^\infty q^3 \mathcal{O}^- \langle \kappa_1 \rangle_\delta \, dq = \frac{16\eta}{3kT} \int_0^{q_{max}} q^3 \mathcal{O}^- \langle \kappa_1 \rangle_\delta \, dq \ , \tag{B.26}$$

because $\langle \kappa_1 \rangle_\delta$ is zero (or neglible) for wave vectors $q > q_{max}$. With Equation B.25 the measured particle size distribution is obtained without a 'fit by eye'.

APPENDIX C

PMMA GEL DATA

Almost every sample of this study could be fitted somehow to a single or double Schulz distribution. In this appendix, data for a sample entirely different from the previous ones are presented. This sample consisted of polymethylmethacrylate gel polymers. The particles are formed by crosslinked polymer chains which do not form a solid 'hard' sphere but rather can be described as a 'hair ball'. These particles contain large amounts of solvent inside, they can swell (dependent on volume fraction) and shrink. Nevertheless these model 'soft' spheres seem to be fairly monodisperse. (They crystallize and are not charge stabilized.) The experimental procedure was similar to the other samples. A dilute sample of these gel particles in benzyl alcohol was investigated at different scattering angles. The intensity and the correlation function were measured from 16 to 130 degrees in 2 degree steps. The duration of each measurement was 200 seconds — shorter than for the other samples. The average intensity of the PMMA Gel particles in benzyl alcohol is shown in Figure 25. Despite the shorter run time at each angle, the correlation functions looked good. The results of the cumulant fit to those autocorrelation functions are shown in Figure 26. The general behavior of the dynamic radius of these particles is similar to the one observed at the other samples: the apparent size shows a maximum when the intensity is at its minimum. There is however one serious difference. The radius corresponding to the static scattering is only 210 nm which is only half the radius of the average dynamic light scattering fit! Because of that reason, the apparent size can not be fit nicely. The size from the dynamic fit does not agree with the static. In Figures 25 and 26 the main fitting criterion was chosen to be the static scattering because both static and dynamic scattering show an extremum in the same angle interval. This
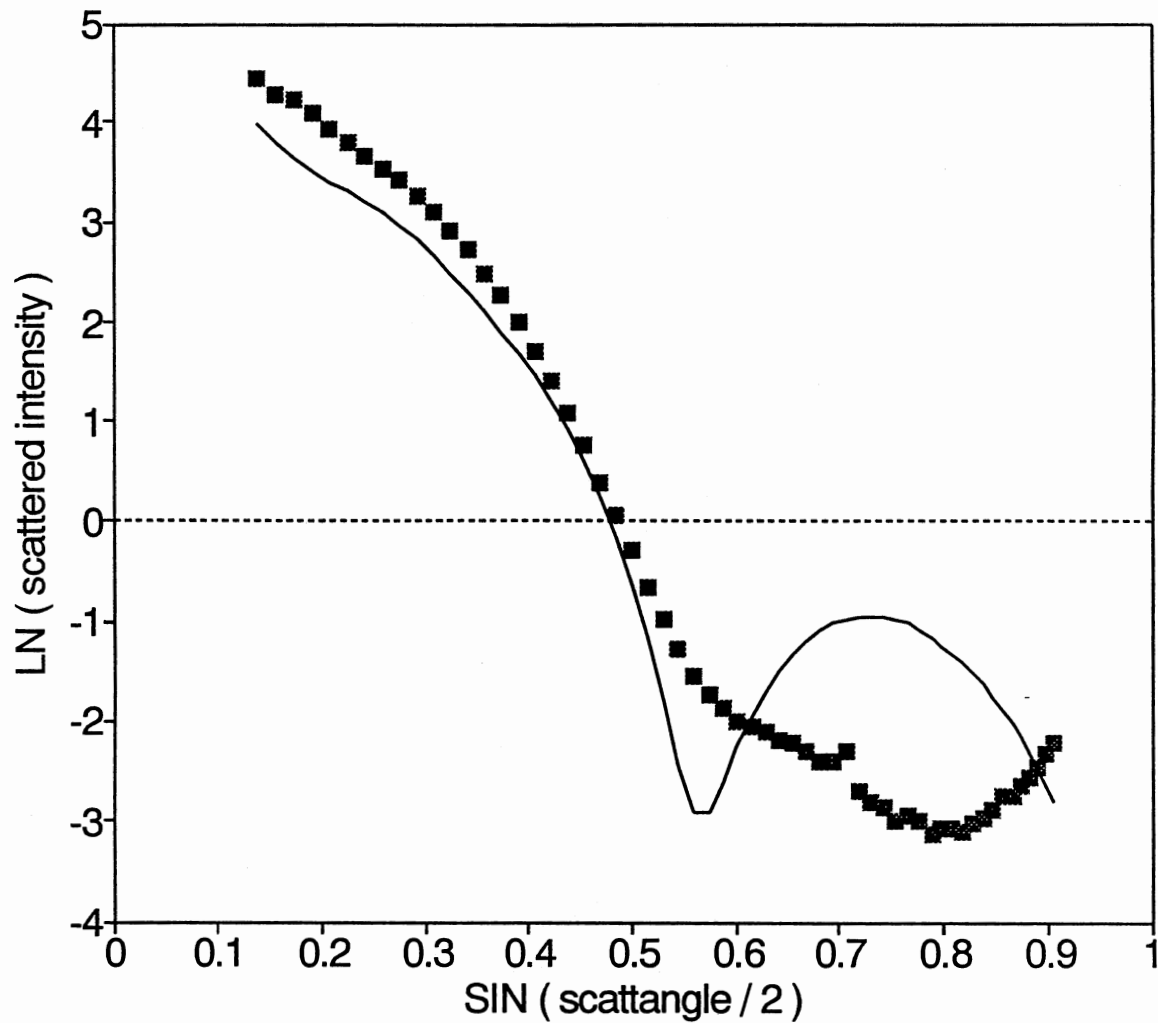
Figure 25. Form Factor of PMMA Gel in Benzyl Alcohol.The natural logarithm of the scattered intensity is plotted versus sin $(\theta/2)$. The fit (solid line) is calculated using $\overline{R_1} = 210$ nm, $\overline{R_2} = 560$ nm, $\kappa = 200$, $Z_1 = 1000$, and $Z_2 = 1000$.
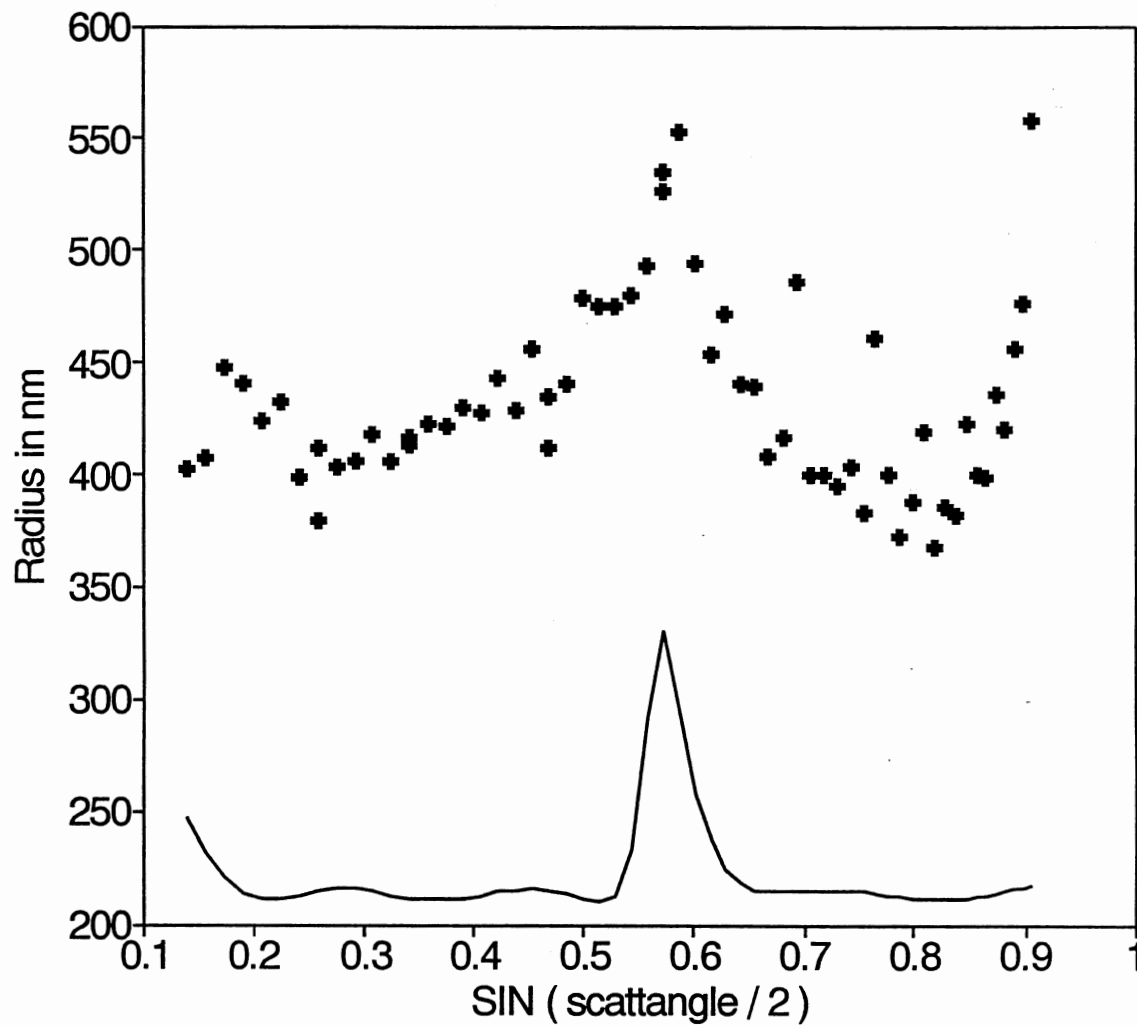
Figure 26. Dynamic Radius versus $\sin(\theta/2)$ of PMMA Gel in Benzyl Alcohol. The fit (solid line) is calculated using $\overline{R_1} = 210$ nm, $\overline{R_2} = 560$ nm, $\kappa = 200$, $Z_1 = 1000$, and $Z_2 = 1000$.

happened with all other samples as well. If the fitting emphasis is placed onto the dynamic radii, this extremum can not be fit. (There are also other extrema where the scattering data are constant, because a form factor for a larger size shows more extrema.) The minima in the form factor do not match as well resulting in two 'bad' fits whereas, with the criterion chosen, only one fit is not good. However this explanation of the scattering of this sample is by no means perfect. In the derivation of the form factors and the apparent sizes, hard sphere properties were used. These PMMA gel particles are *not* hard spheres. Starting from different assumptions, it might be possible to explain the results quantitatively. It should however be noted that even these particles show a higher apparent size at those angles where the scattered intensity is small.

VITA

ULF NOBBMANN

Candidate for the Degree of

Master of Science

Thesis: LIGHT SCATTERING FROM MICRON SIZED PARTICLES

Major Field: Physics

Biographical:

> Personal Data: Born in Nienburg/Weser, Germany, June 4, 1966, the son of Friederich and Siegrid Nobbmann.

> Education: Graduated from Gymnasium Hindenburgschule, Nienburg, Germany, June, 1985; passed 'Diplomvorprüfung im Studiengang Physik' from Universität Hannover, Hannover, Germany, October, 1988; completed the requirements for the Master of Science Degree at the Oklahoma State University, Stillwater, Oklahoma, December, 1991.